![Chalmers University of Technology logo]

CHALMERS
UNIVERSITY OF TECHNOLOGY

Thermal Characterization of a Cylindrical Li-ion Battery Cell

Master's thesis in Electric Power Engineering

Guilherme Matheus Todys
S M Shadhin Mahmud

MASTER'S THESIS 2020

Thermal Characterization of a Cylindrical Li-ion Battery Cell

Guilherme Matheus Todys
S M Shadhin Mahmud

Thermal Characterization of Cylindrical Li-ion Battery Cell
Guilherme Matheus Todys
S M Shadhin Mahmud
Department of Energy and Environment
Chalmers University of Technology

Abstract

The operating temperature of Li ion batteries is one of the main aspects to consider when analysing the battery's performance. The battery's internal temperature interferes with important characteristics of the battery, such as lifetime and overall performance. In order to avoid any issues related to the thermal behavior of the batteries, efficient thermal management systems are required. Therefore, a thermal characterization of Li ion cells is necessary to provide the thermal parameters needed for further battery's thermal studies, and the development of adequate thermal management systems. This thesis work presents a thermal characterization of a Tesla cylindrical Li ion cell, describing methods for the measurement of the specific heat capacity, axial thermal conductivity and radial thermal conductivity.

All the experiments were implemented utilizing a custom-made isothermal heat conduction calorimeter (IHCC). The calorimeter was originally designed to work with prismatic and pouch cells. Therefore, all the process related to the design modifications, in order to adapt the calorimeter to work with cylindrical cells, is also described in this thesis. The methods developed were validated utilizing a Polyoxymethylene (POM) sample with the same dimensions of 21700 cylindrical cell.

Some issues related to heat leakage were faced when performing the experiments, and they were overcome by improving the calorimeter set-up. Finally, the results obtained from the measurements presented reasonable values and a very good precision, being an important contribution in the thermal characterization of cylindrical Li ion cells.

Keywords: Thermal conductivity, Thermal characterization, Specific heat capacity, cylindrical cell, Li ion battery cell, Isothermal Heat Conduction Calorimeter, Tesla cylindrical cells.

Acknowledgements

Contents

Contents

1

Introduction

One of the main challenges faced by the society worldwide is to align its rapid expansion and development with sustainability [8]. High levels of CO_2 emissions are responsible for contributing to environmental problems around the globe, such as climate change and air pollution, and can be associated with the operation of internal combustion engine vehicles (ICEs) [6, 8]. In this scenario, electric vehicles (EVs) have become popular inside of the automotive industry as a promising solution for these issues [6]. Due to its high power and energy density, as well as stable operation voltage and durability, lithium ion batteries (LIBs) were chosen as the energy storage devices used in EVs [5, 6]. To control the operating temperature is crucial to secure the proper performance and lifetime of lithium ion batteries, making thermal management a key factor to be considered when working with LIBs. [3, 4, 5]

1.1   Background

Operating temperature is one of the main concerns when working with lithium ion batteries [12]. Internal and surface temperature difference and nonuniform temperature distribution, caused by a poor thermal conductivity, are problematic characteristics that contribute to increase the complexity of thermal management [15]. When the battery is in operation, heat is generated due to the battery internal resistance associated with the charge/discharge rate, which is responsible for a gradual increase of the battery's temperature [16]. If this increase of temperature is not controlled, and the battery temperature is not maintained within a safe range of 20°C – 40°C, the consequences can be low performance, lifetime reduction, and even, in more critical situations, thermal runaway [9, 12]. To increase thermal stability and maintain the operating temperature inside of the mentioned range, thermal management systems must be designed and utilized. To do so, the battery is described using thermal models, so it can be studied in terms of thermal behaviour. These models consider the battery's thermal properties, such as heat conductivity and specific heat capacity. Therefore, to obtain the most optimize thermal management system, it is necessary to have a good estimation of the battery's thermal properties.

1.2   Previous Work

In this segment, previous work regarding the thermal characterization and other aspects related to the thermal properties of the Li-ion battery is briefly described. The works below lead to operate the thermal parameters measurement and created

a scope of doing this thesis work .

From Chen, et.al.[27], the heat generation in a prismatic Li-ion cell ($A213LiFeP0_4$) was measured by utilizing an isothermal heat conduction calorimeter. The heat generation of a cell was measured under a wide range of 0.25C and 3C and the operating temperature was 30°C and 40°C. Heat generation rates were measured. The calorimeter was designed for prismatic cells, that was placed in direct contact between two slabs of high-density polyethylene (HDPE). This setup was placed between two aluminum and inside an isothermal bath of a 50-50 mixture of ethylene glycol-water. Two thermocouples were used as one in each HDPE slab and approximately at a depth equal to the center of the battery. Besides, those two additional thermocouples were attached over each battery surface. The main thought behind this kind of setup was to evaluate the heat generated in the batteries from the temperature measurements by assuming one-dimensional heat transfer in the HDPE slab. The results had an inaccuracy in the measurement of the heat generation against a known input heat from heaters of approximately 20% in this setup. Also, the method failed to measure any thermal parameters of the Li-ion cell. Therefore, the measured heat generation can only be used to estimate the capacity of the cooling system and not estimate the internal temperatures of the battery.

Löwen,et.al.[29] measured the heat capacity of liquid and metal samples was measured by using the dynamic correction constant of the calorimeter. Tian correction equation was used to correct the output signal from heat flow sensors in the time domain. The value of the dynamic correction factor signifies the thermal mass of the sample and can be used for the measurement of specific heat capacity of samples. Within an uncertainty of less than 4%, heat capacity was measured by this method. The calorimeter had a sample holder cup which was an issue for samples with low conductivity, especially liquids as compared to metals samples.

Byden,et.al.[11] developed a method to determine the specific heat capacity of Li-ion cells. That method was established by utilizing simple battery laboratory equipment. This method worked for cylindrical, prismatic and pouch cells within a range of capacity 2.5 Ah to 10Ah. The result was validated by using a calorimeter with a maximum error of 3.9%. The temperature was kept within a specific limit. Internal thermal resistance was also measured from this method. This model only can be used to obtain the surface temperature of the cells at C rates over 1C.

Lidbeck et.al. and Syed et.al. [28] developed methods to determine the thermal characterization of the pouch and prismatic Li-ion cell. Thermal conductivity and specific heat capacity were measured. Besides, the heat generated from the cell was measured for different load cycles. Measured thermal properties are also used as an input in a simulation model for obtaining the peak temperature during charging and discharging. All the experiments for measuring thermal parameters were performed by using a custom-designed modified calorimeter (fitted for the pouch and prismatic cells). Calorimeter setup and the method of determining the specific heat capacity and thermal conductivity were validated by available sample materials. Heat gen-

eration and specific heat capacity were measured successfully for both cells. Also, the thermal conductivity of the pouch cell was measured successfully. On the other hand due to conduction through Aluminium casing the method was inapplicable for prismatic cells.

1.3 Purpose

The purpose of this master thesis work is to develop experimental methods for complete thermal characterization of cylindrical Li-ion cells. Furthermore, the target is to evaluate and redesign an Isothermal Heat Conduction Calorimeter (IHCC) that is already utilized for thermal characterization of prismatic and pouch cells. The methods will be developed aiming to measure the thermal parameters of cylindrical Li-ion cells, such as axial and radial thermal conductivities, and specific heat capacity.

1.4 Scope

The main focus of this work is to experimentally determine the thermal parameters of a cylindrical Li-ion cell. The experiments were conducted at Volvo GTT battery lab., where an IHC was provided as well as all the other necessary equipment. The design of the IHC was changed in order for it to enable the testing of 21700 cylindrical cells. All the methods presented were verified utilizing samples with well-known thermal characteristics and parameters. In addition, all the tests were conducted in a room temperature of 20ºC, and the effects of the cell's state of charge and state of health on the temperature parameters were not considered.

1.5 Environmental & ethical aspects

Nowadays, environment and ethics are two of the major issues in battery industry. These two aspects are elaborated in these thesis work. The growing demand for EVs and HEVs in the vehicle industries have led to the discussion where the automobile industries are aiming for zero-emission from these vehicles. Li-ion batteries, which is an essential part of EVs and HEVs, plays a significant role in these aspects. To this extent, improving the lifetime of these battery, extending their sustainable production and recycling is the demand of the current world [25]. Operating conditions will be optimized for extending the batteries lifetime. It means the thermal management is very important to extend the battery lifetime for environment aspect. For safety issue, the temperature must be controlled and regulated to increase the lifetime. Batteries are not replaced, but it would be better utilization for both resources and fewer effects on the environment [27].

On the other hand, ethical issues are normally considered in experimental thesis work. IEEE code of ethics has been used for this thesis work. First code of ethics [26] from this experiment, the health, safety and welfare of the public may be af-

fected. Wrong utilization of thermal management systems in any applications may be dangerous and cost-effective. Thus, It is vital to improved thermal parameters and design thermal management in a user-friendly way. The third code of ethics is on line with this thesis perspective [26]. Taking ethical decisions regarding experimental thermal results are always tricky owing to the measurement errors that shall be taken into account. Best results are chosen and presented with pictures. In addition, the second and eight code of ethics in collaboration with the people are involved with this experiment [26].

2

Theory

2.1 Li-ion cell

Since Li-ion cells are a type of electrochemical cells, to understand its working principle, it is necessary to understand how an electrochemical cell operates. An electrochemical cell converts chemical energy to electrical energy and the other way around. This type of cell can also be classified in two groups: primary cells and secondary cells. A cell is classified as a primary cell when it only converts chemical energy into electrical energy (galvanic nature), this cell is thus non-rechargeable. On the other hand, a secondary cell, which is the case of a Li-ion cell, can both convert chemical energy to electrical energy and electrical energy to chemical energy (both galvanic and electrolytic nature), and is thus rechargeable [8].

The most elementary design of an electrochemical cell consists of a positive and a negative electrode, a separator and electrolyte. The electrodes are considered as active components, and all the other elements are considered as non-active components. During charging and discharging, electrochemical oxidation and reduction reactions, also called as redox reactions, will occur on the electrodes. The result of such reactions is the transfer of both electrons and ions from one electrode to another. An external circuit is responsible to provide a path for the electrons to flow between the electrodes, and the ions will be transferred through the separator and electrolyte [8]. A schematic of a Li-ion cell structure can be seen in Figure 2.1

A brief description of the cell components is presented below:

Positive electrode (cathode) and negative electrode (anode): An electrode is composed of ionically and electrically conducting material, that can be either metallic or of insertion type. When it comes to rechargeable batteries, insertion electrodes are most commonly used [8]. Separator: In most cases, a separator is a membrane soaked in electrolyte, and its function is to prevent any direct contact between the electrodes. The separator material must provide both high ion conductivity and good electrical insulation [8].

Electrolyte: In general, electrolytes can be described as a solution of one or several salts dissolved in one or several solvents. The main purpose of electrolyte is to provide a path for the ions to flow from one electrode to another, but not conduct electrons. Therefore, like the separator, it must have both high ion conductivity and
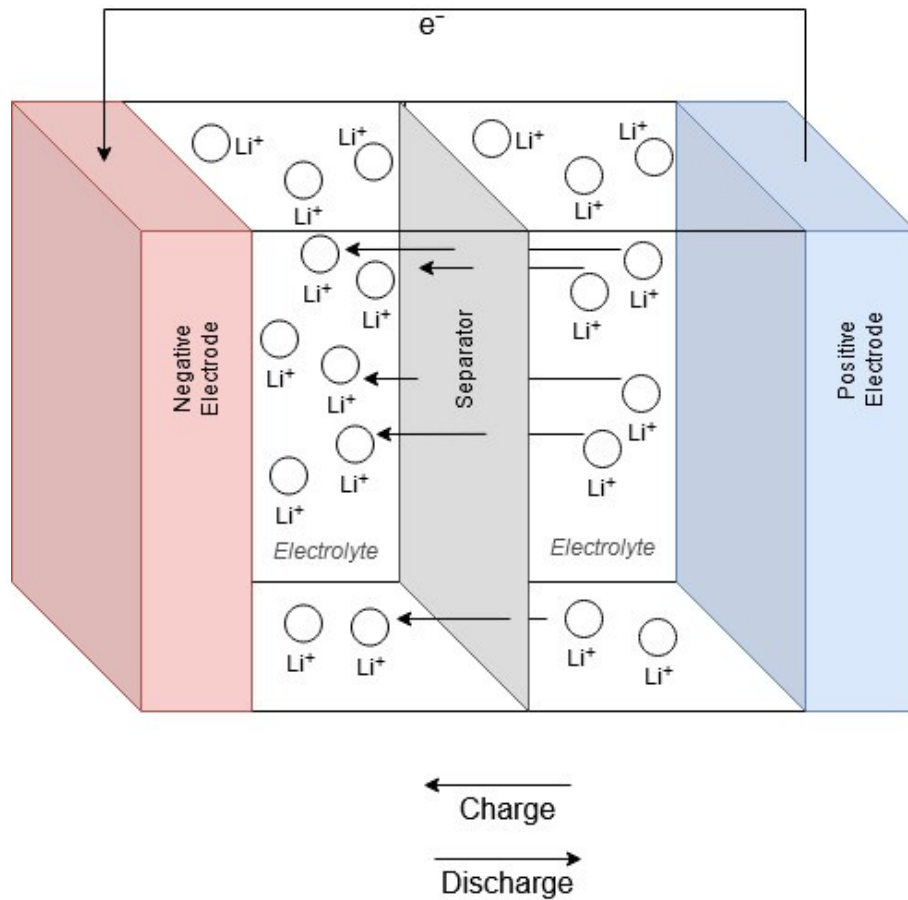
Figure 2.1: Li-ion cell structure schematics.

good electrical insulation [8].

Most Li-ion cells have the same material composition for the negative electrode (graphite) and for the electrolyte (1M $LiPF_6$ in EC/DCM). However, there are several options to chose from when it comes to the material composition of the positive electrode. The positive electrode composition can be considered as the crucial choice to be made when deciding the overall characteristics of the cell and its performance. There is no such a thing as a perfect or ideal material that will meet all requirements for all kinds of applications. Therefore, a suitable material must be chosen, in order to achieve the requirements of a given application in the best way as possible [8]. Table 2.1 presents a relation between some options of materials for the positive electrode and its characteristics, grading it from 1 (lowest grade) until 5 (highest grade) [7].

Each cell has a capacity (Q), which will vary depending on its chemistry and other physical characteristics. The capacity of a cell is usually expressed in Ampere-hour [Ah]. Another important parameter to be considered to operate the cell is the C-rate. The C-rate can be understood as the current normalized to cell capacity, therefore, a C-rate equals to 1 means that the battery will be cycled with such a current that

Table 2.1: Some options of materials for the positive electrode.

Cell Chemestry	Specific Energy	Specific Power	Safety	Performance	Life span	Cost
Lithium-nickel--cobalt-aluminium (NCA)	4	4	2	3	3	2
Lithium-nickel--manganese-cobalt (NMC)	4	3	3	3	3	3
Lithium-manganese--spinel (LMO)	3	3	3	2	2	3
Lithiumtitanate (LTO)	2	3	4	4	5	1
Lithium-iron-phospate (LFP)	2	3	4	2	5	3

it will take one hour to charge or discharge it. Additionally, battery cells can be designed to be energy optimized or power optimized, which mainly depends on the application required. A cell that is designed to be mainly an energy optimized cell will have a very good energy content, however the power content of this cell will be low, and vice-versa. Moreover, energy optimized cells should only be operated at low C-rates, and power optimized cells can be operated at high C-rates. Figure 2.2 presents a Ragone plot which is very useful to better understand the relation between energy optimized cells, power optimized cells and C-rate. In the figure, points "E" and "P" represent, respectively, maximum energy density and maximum power density, and point "X" is the optimal state, which represents both maximum energy and power content, this point, however, is unachievable.[8]
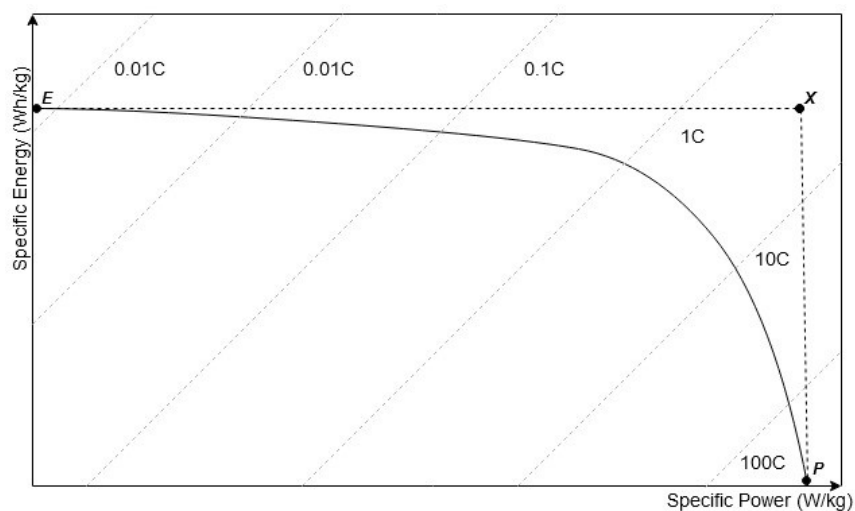
Figure 2.2: Ragone plot of an energy-optimized and power optimized cell.

2.2 Cell design

Li-ion cells are hermetically sealed in casings, commonly based on aluminium or plastics, which can have different formats. Depending on the format chosen, the battery cell shall have different performance characteristics and limitations. When it comes to electrical vehicles, three classes can be listed: cylindrical, prismatic and pouch. [8]

2.2.1 Cylindrical cell

The internal arrangement of a cylindrical cell resembles a jelly roll, and its capacity increases as its diameter increases (thicker cells have higher capacity and vice versa). The nomenclature for this group is based on the diameter and the height of the cylinder, e.g. a 21700 cell has a diameter of 21 mm and a height of 70 mm. The main advantage of this format is its simple production, and its main downsides are temperature management and packaging issues. Therefore, a trade-off between thermal performance and cell capacity must be done is order to determine its size. The cylindrical cell structure is shown in Figure 2.3.
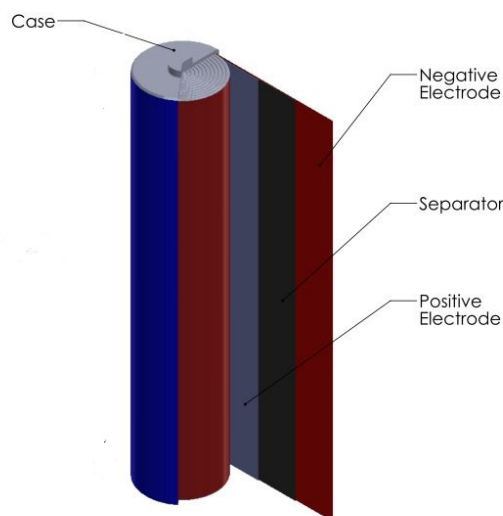
Figure 2.3: Cylindrical cell's structure and composition.

2.2.2 Prismatic cell

The two most common ways to produce a prismatic cell are stacked or wound, and it depends on the desired cell characteristics. Regarding the nomenclature, usually, the format is given in terms of thickness, width, and length. Prismatic cells have a hard casing, usually made of Aluminium, which is the main difference between prismatic and pouch cells. High density batteries can be build based on prismatic cells, however thermal management can be a problem if the packaging is not properly designed. Adjacent cells may heat each other, due to its heat dissipation, so thermal

management devices are placed between the cells to control the temperature of the pack [8]. The prismatic cell structure is shown in Figure 2.4.
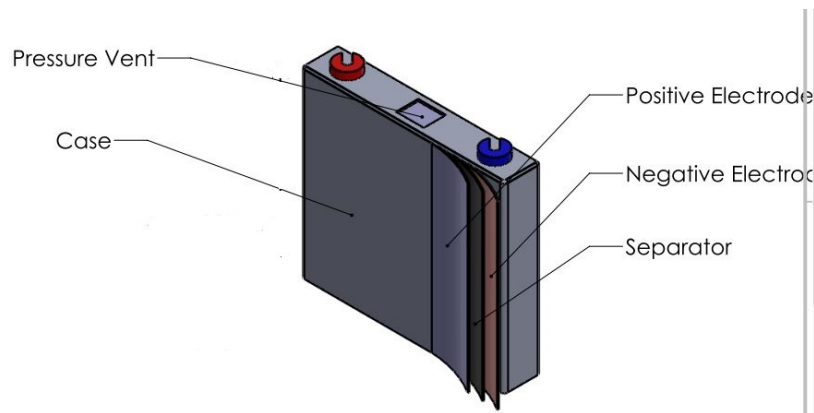
Figure 2.4: Prismatic cell's structure and composition.

2.2.3 Pouch cell

Prismatic or flat in the basic format, pouch cells are encapsulated in a soft package casing, most common made of polymer-laminated aluminium foil, and its electrodes are typically stacked or Z-folded, depending on the capacity of the cell and other operation characteristics. Heat or ultrasonic welding are utilized in the package sealing. Similar to what happens with prismatic cells, thermal management devices are placed between the cells in a pack, in order to ensure a safe operation [8]. The pouch cell structure is shown in Figure 2.5.
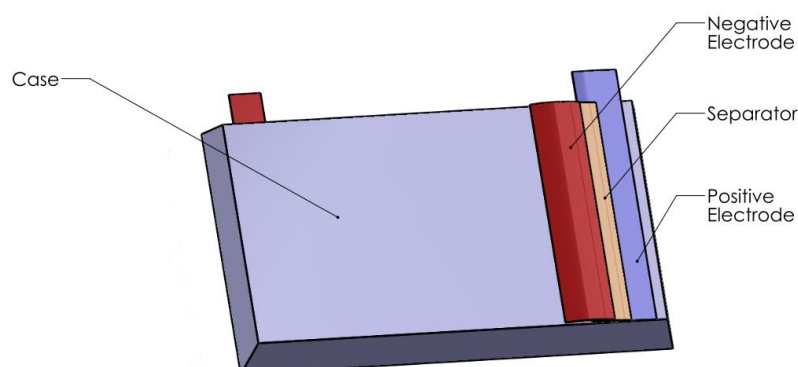
Figure 2.5: Pouch cell's structure and composition.

2.3 Heat Transfer

In a general way, heat transfer can be defined as the transport of thermal energy generated by temperature difference in space [1]. Therefore, whenever a temperature difference between two points in space exists, heat transfer will occur [1]. Heat can be transferred in three different modes: conduction, convection and radiation. The term conduction refers to the heat transferred across a stationary medium, solid or fluid, whenever a gradient of temperature exists across it. Convection is used to denominate the heat transfer that occurs between a fluid in movement and a solid, considering a temperature difference between them. Lastly, the radiation takes place when two surfaces are at different temperatures, and the heat transfer is established through electromagnetic waves [1]. Figure 2.6 illustrates the three different heat conduction modes mentioned.
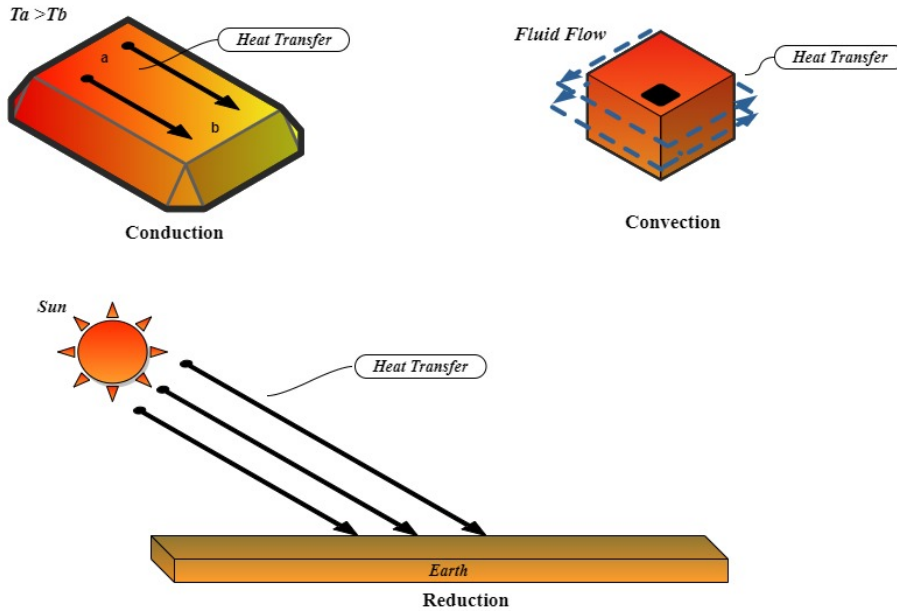
Figure 2.6: Heat conduction modes.

The heat diffusion equation, also known as the heat equation, is defined as

$$\frac{\partial}{\partial x}\left(k\frac{\partial T}{\partial x}\right) + \frac{\partial}{\partial y}\left(k\frac{\partial T}{\partial y}\right) + \frac{\partial}{\partial z}\left(k\frac{\partial T}{\partial z}\right) + \dot{q} = \rho c_p \frac{\partial T}{\partial y} \tag{2.1}$$

where k is the thermal conductivity $[W\,m^{-1}\,K^{-1}]$ dependent on Cartesian coordinates x, y and z, T is the temperature $[K]$ in a certain coordinate (x,y,z) within the medium, C_p is the specific heat capacity [J kg^{-1} K^{-1}], ρ is the mass density, $\dot{q}$ is the heat transfer rate per unit of volume and t is time. Equation (2.1) is consider as the starting point to perform a heat conduction analysis. Furthermore, the distribution of temperature, $T(x, y, z)$, as a function of time can be achieved from its solution [1]. Considering cylindrical coordinates and applying the proper changes in

(2.1), the heat equation can be written as

$$\frac{1}{r}\frac{\partial}{\partial r}\left(kr\frac{\partial T}{\partial r}\right) + \frac{1}{r^2}\frac{\partial}{\partial \phi}\left(k\frac{\partial T}{\partial \phi}\right) + \frac{\partial}{\partial z}\left(k\frac{\partial T}{\partial z}\right) + \dot{q} = \rho c_p \frac{\partial T}{\partial y} \tag{2.2}$$

Both (2.1) and (2.2) can be simplified depending on the conditions considered for the control volume. For example, considering steady state condition, the amount of energy stored cannot vary, thus (2.1) will become

$$\frac{\partial}{\partial x}\left(k\frac{\partial T}{\partial x}\right) + \frac{\partial}{\partial y}\left(k\frac{\partial T}{\partial y}\right) + \frac{\partial}{\partial z}\left(k\frac{\partial T}{\partial z}\right) + \dot{q} = 0 \tag{2.3}$$

Therefore, modifications of the heat diffusion equation are often seen, resulted from its application in different circumstances and situations.

2.4 Calorimeter

The Calorimeter is a heat measuring device consists of vessel or cell which is in contact with the sample. Surrounding of the calorimeter is called a shield or thromostat which can be more than one to isolate the calorimeter. Calorimeter follows the heat equation described by Zielenkiewicz and Margas[17] as

$$P(t) = G(T_c(t) - T_0(t)) + C\frac{dT_c(t)}{dt} \tag{2.4}$$

Two different calorimeters can be found on the basis of temperature gradient between shield and vessel, Adiabatic and Non-adiabatic. Adiabatic calorimeters can be divided in two subcategories, with constant shield temperature $T_0(t)$ named adiabatic isothermal and temperature changes with time $T_0(t)$ named adiabatic-nonisothermal calorimeters. Nonadiabatic calorimeters have two subdivision, constant shield temperature $T_0(t)$ called isoperibol and temperature $T_0(t)$ changes with time. Isoperibol calorimeter has a temperature gradient stable with time which is also known as non-adiabatic isothermal calorimeters. One example of this type is scanning calorimeters and the custom-made calorimeter in battery lab at Volvo GTT.

2.4.1 Isothermal heat-conduction calorimeter

Isothermal calorimeter shield has a constant temperature. General construction procedure of this calorimeter is shown in figure 2.7

In between the two heat sensor(thermopiles), the sample in the cup is placed. The thermopiles are in direct contact with heat sinks (made from aluminum and has internal coolant circulation) maintained at a constant temperature. When heat generated or absorbed in the sample, the temperature change is related to the stable heat sink temperature conditions. This difference between temperature starts the heat flow through the sensors that measure the heat. Also the sensors create voltage that has to be converted into the thermal power.
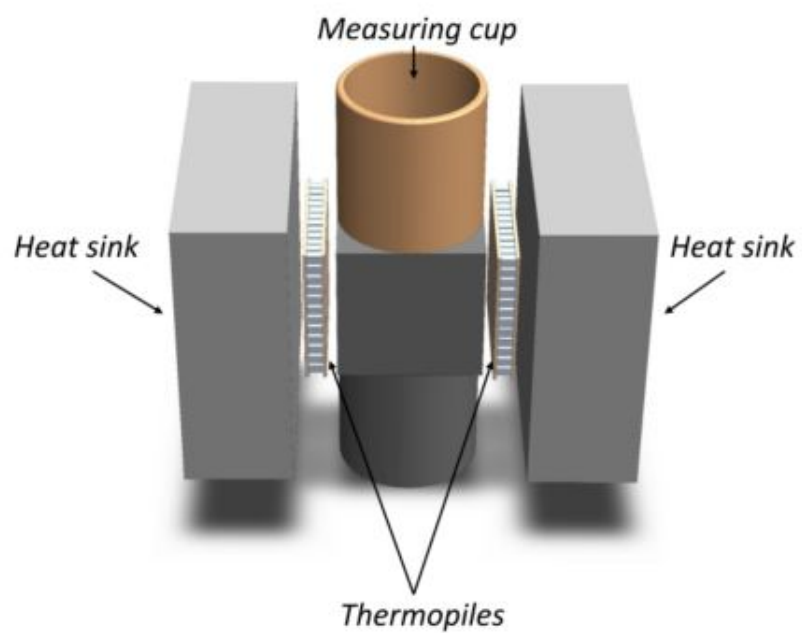
Figure 2.7: Isothermal Heat conduction calorimeter [28].

3

Case setup

In this chapter, the IHC calorimeter design is presented and described, as well as its construction and calibration procedure. The set-up utilized for data acquisition is also presented in this chapter.

3.1 Experimental setup

The isothermal heat conduction calorimeter used in this master thesis belongs to Volvo Group Trucks Technology (GTT). This IHCC was developed in past studies to be employed in thermal characterization of pouch and prismatic Li-ion cells [2]. The calorimeter consisted of two parts, side A and side B. Each part, or side, had its heat sink, composed of two aluminum plates with water flow channels machined into them. The heat sinks were fixed to pressure plates that should be in close contact with the studied sample. Therefore, the sample was sandwiched by both pressure plates. Between the pressure plates and the heat sinks, there were six heat flow sensors, called thermopiles, on each side, totalizing twelve heat flow sensors for the whole calorimeter. PT100 temperature sensors were also placed in drilled holes located in the side of both heat sinks and pressure plates. A picture of the described design is shown in Figure 3.1.
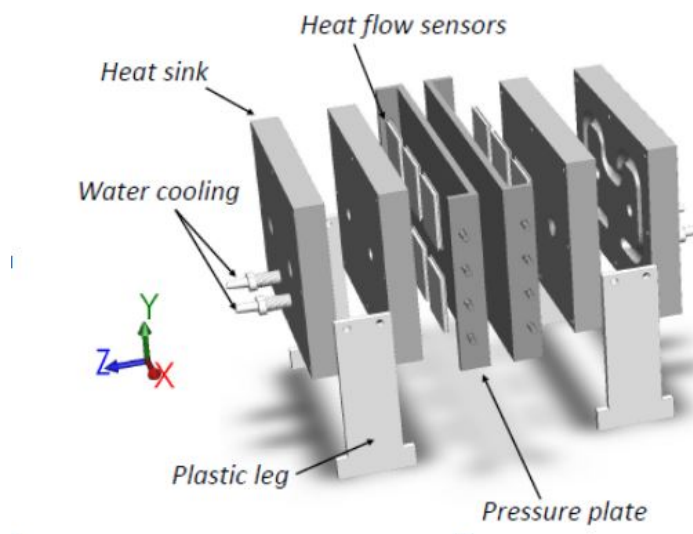
Figure 3.1: Old calorimeter set-up [2].

The temperature readings were recorded by PICO-104 Data Logger [23], and the heat flow measurements were recorded by both PICO-104 Data Logger and GAMRY 3000 Refence [22]. On any occasion that a source of power was needed, in order to supply a heater or even a Li-ion cell, the GAMRY 3000 Refence was utilized. The technical specifications of both devices are presented in Table 3.2. The Julabo F25MA thermal bath [21] was utilized to control the temperature of the water flowing through the heat sinks. Lastly, The whole set-up was placed inside of an insulation box made of Therma TW50 insulation plates [24].

Table 3.1: GAMRY 3000 Refence and PICO-104 Data Logger technical specifications [2].

GAMRY 3000 Reference	
Operation limits	± 15 V; 3.0 A or ± 30 V; 1.5 A
Potential applied accuracy	$\pm$ 1 mV $\pm 0.2\%$ of setting
Potential measured accuracy	$\pm$ 1 mV $\pm 0.2\%$ of reading
Current applied/measured accuracy	± 5 pA $\pm$ 0.05% of range
PT-104 Data Logger	
Compatibility	Works with PT100 and PT1000 sensors
Accuracy (unit at 23 ± 2 °C)	0.015 ◦C +0.01% of reading
Resolution	0.001 ◦C

The main concept behind the mentioned set-up is that whenever heat flows from, or to, the cell, it will be measured by the thermopiles located between the preasure plates and the heat sinks. Furthermore, an additional calorimeter was added to the system, in order to work as a source of reference signals from the measurement equipment, being applied to off-set and bias corrections. Therefore, the whole system was composed by 2 calorimeters: calorimeter S, were the sample was placed, and calorimeter R, used as a reference calorimeter. To perform the signal correction process, the signals average values from side A and B of calorimeter R, of both heat flow and temperature measurements, were subtracted from the respectively signals of calorimeter S.

Since the previous calorimeter was not designed to work with cylindrical cells, design changes were needed. After analyzing the old design carefully, it was decided to change only the pressure plates configuration, to make use of as many parts of the old design as possible [2]. Since the previous designed was projected to work with prismatic and pouch cells that were significantly bigger than a 21700 cylindrical cell, one of the first ideas was to utilize the old design, that could handle one prismatic or pouch cell at a time, to work with two or three cylindrical cells simultaneously. In other words, the idea was to utilize the same heat sink structure coupled to two or three pairs of pressure plates that would hold a cylindrical cell each. Taking by base a 21700 cylindrical cell, a new configuration of pressure plates was designed. The final concept for the plates can be seen in Figure 3.2

The height of the plates is 78 mm, the length is 40mm, the thickness is 12.5 mm
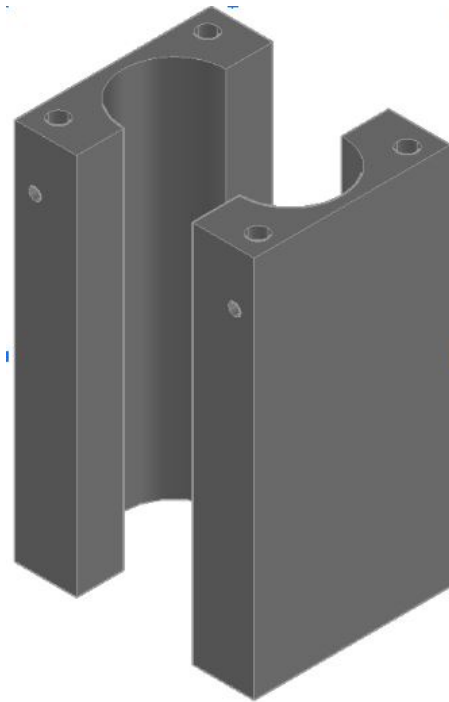
Figure 3.2: Pressure Plates.

and the radius of the cylinder is 10.5 mm. The cross-section dimensions of the heat sinks are 165x120 [mm]. Therefore, it was decided to utilize two sets of pressure plates for the new design, attached on the extremities of the heat sink. Between each pressure plate and heat sink, two heat flow sensors were fixed, summing up a total of eight heat flow sensors, considering both sides of the calorimeter. Additionally, every pressure plate has a temperature sensor located inside of a hole made in its side. More details about the sensors and measurement equipment will be presented in section 3.2. The whole design is held together with the help of two tension spring holders, which are located inside of holes made in the heat sink plates. The new design of the calorimeter can be seen in Figure 3.3. In order to minimize the heat losses to the surroundings, and to maintain the condition of an isothermal environment, the IHC is kept inside of a box with glass wool insulation. In addition to that, an isothermal bath system, JULABO F25MA, was utilized to control the temperature of the heat sinks.

3.2 Calibration

Heat flow is quantified in Watts [W], however, the heat flow sensors utilized in this set-up provide the output signal in Volts [V]. For this reason, and also to check the measurement range and the accuracy of the calorimeter, a calibration procedure is needed. Through the calibration, the calibration constant ((ϵ)) is obtained, which is a proportionality constant responsible for converting the signal output from [V] to [W]. To perform this procedure, a previously known amount of power must be applied to the calorimeter, and the output signals from the sensors must be recorded.

Therefore, a calibration heater specifically for this set-up was built.

3.2.1 Calorimeter Setup

The set-up utilized to perform the calibration had the same design as presented in section 3.1. Furthermore, the custom-made calibration heater was placed in a pair of pressure plates (calorimeter S), while the other pair (calorimeter R) was left empty. During the procedure, the heat flow and temperature of each set of pressure plates were recorded. A piece of Styrofoam was also included in the gap between the two sets of pressure plates, to provide more thermal insulation. The complete assembled set-up can be seen in Figure 3.3.
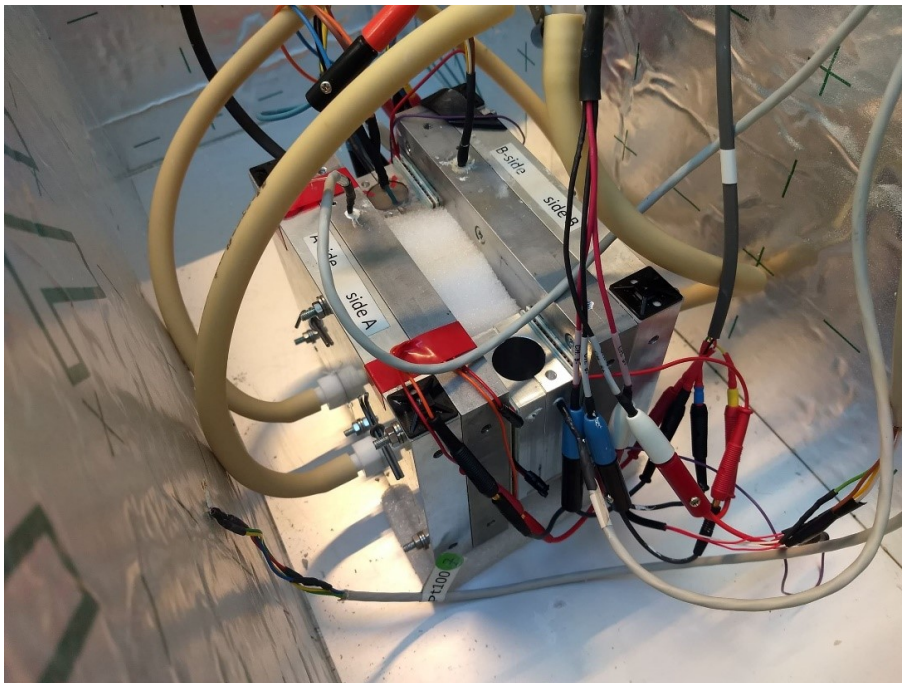
Figure 3.3: Calibration setup

3.2.2 Calibration Heater

As mentioned in sections 3.2 and 3.2.1, a custom-made heater was utilized in the calibration. The heater is composed of a 10 $[\Omega]$ resistor, maximum power of 10 $[W]$, covered by concrete in the shape of a 21700 cylindrical cell. Concrete was utilized in order to provide the heater a shape as similar as possible to a 21700 cylindrical cell, as it can be easily molded for this purpose. Four wires were connected to the heater terminals, two at each terminal, so it could match a 4-wire measurement configuration, ensuring a high precision for measuring the input power of the GAMRY 3000 reference. The heater is present in Figure 3.4

Figure 3.4: Calibration Heater

3.2.3   Calibration Constant

To perform the calibration procedure, four different heater power levels were chosen: 0.1 [W], 0.4 [W], 2.5 [W], 4.9 [W]. Additionally, the calibration was implemented for two values of heat sink temperature: 20°C and 30°C. Different power and temperature levels were tested to analyze the variation of the calibration constant with the input power and temperature. Figure 3.5 shows the heat flow and temperature readings, considering a heat sink temperature of 20°C, while Figure 3.6 shows the same information considering a heat sink temperature of 30°C.

Regarding the heat flow, it becomes evident that there is a higher heat flow through pressure plate A than through pressure plate B. One of the reasons for that could be that the resistor is not located in the exact center of the heater, since it could be moved during the process of adding concrete to form the cylindrical shape. Therefore, the resistor could be closer to pressure plate A, resulting in a higher heat flow through that plate. Moreover, analyzing the temperature curves, it is possible to notice that, as expected, pressure plate A has a higher temperature than pressure plate B, and both heat sinks were able to maintain their temperatures around the defined values (20°C or 30°C).
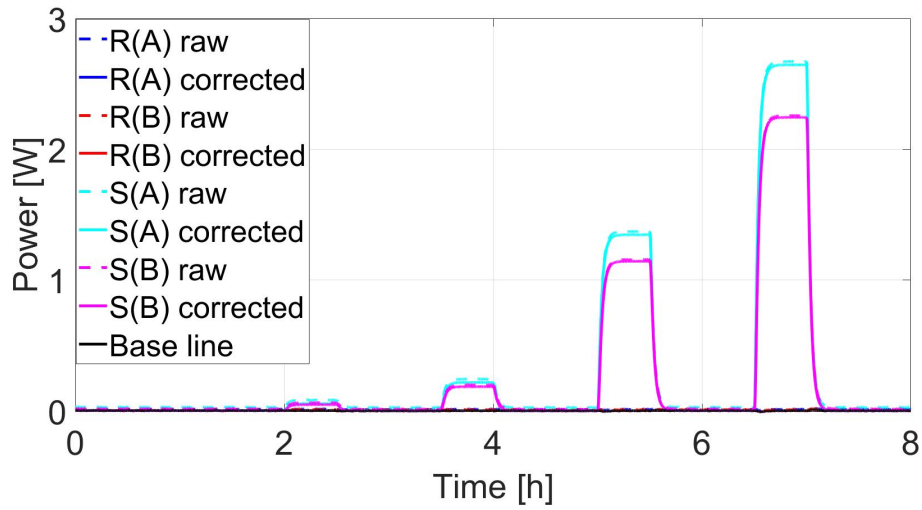
(a) Measured heat flow signals (20°C).
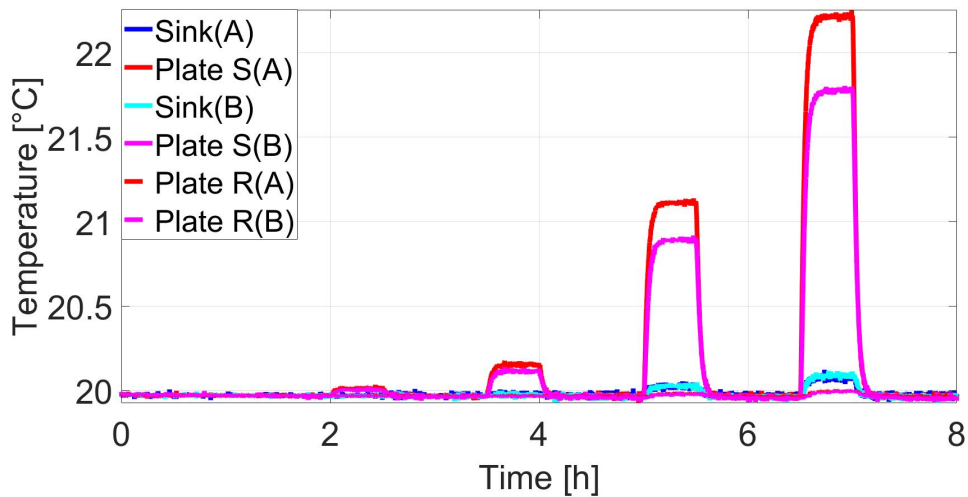
(b) Measured temperature signals (20°C).

Figure 3.5: Measured heat flow and temperature sensors output considering a heat sink temperature of 20°C.

Table 3.1 shows the calibration results considering all the power levels applied and the two different heat sink temperatures. Analyzing Table 3.1, it becomes evident that ε has a small deviation when it comes to power level, with 2.3% as the largest deviation between the highest and lowest value of ε. Therefore, it is possible to conclude that the calibration constant is not strictly dependent on the power level. Moreover, the variation of regarding the two different calibration temperatures was low as well, which is always below 6%. Thus, the calibration constant does not have a significant dependency on the temperature.
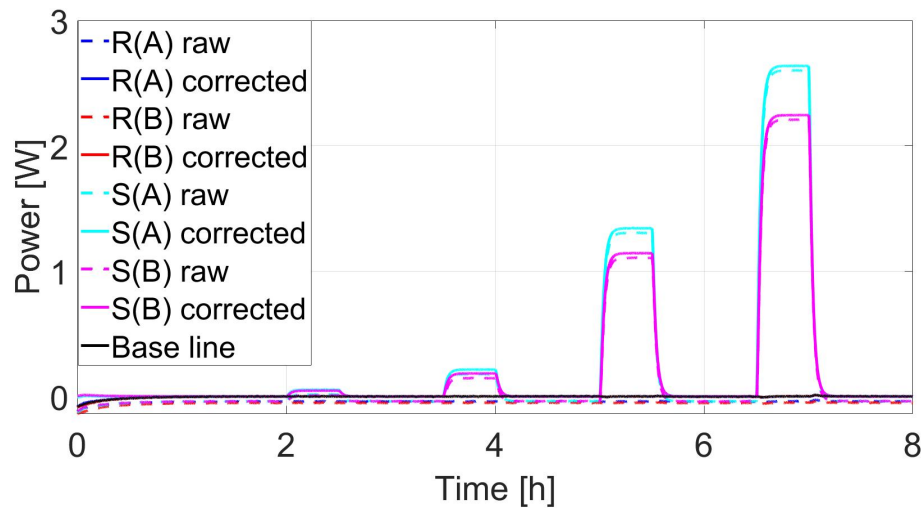
(a) Measured heat flow signals (30°C).
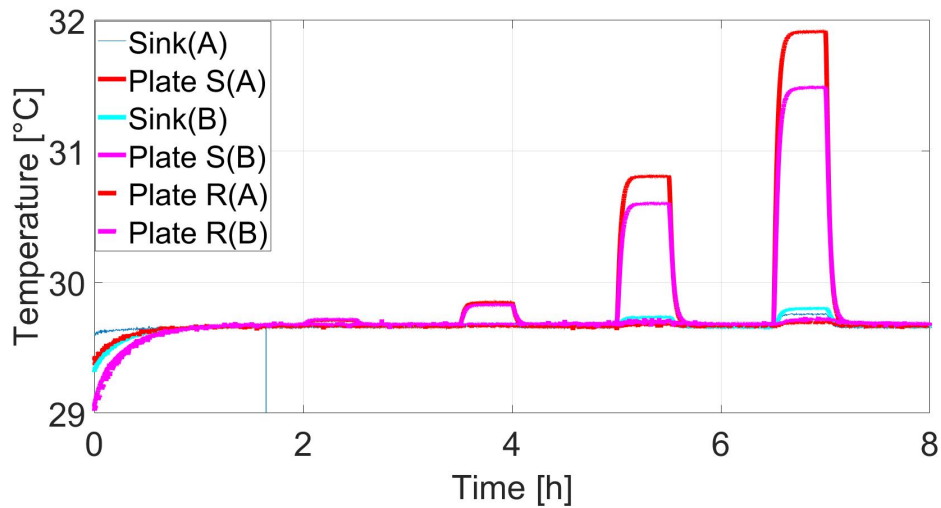
(b) Measured temperature signals (30°C).

Figure 3.6: Measured heat flow and temperature sensors output considering a heat sink temperature of 30°C.

Table 3.2: Obtained values of the calibration constant.

	T = 20°C	T = 30°C	
Power [W]	**Cali. Coef.(ϵ)[W V^{1}]**	**Cali. Coef.(ϵ)[W V^{1}]**	$\epsilon[\%]$
0.1	57.67	59.5	3,17
0.4	57.64	59.3	2.88
2.5	57.73	59.3	2.72
4.9	57.82	59.4	2.73
Average value	57.72	59.38	2.88

3.2.4 Validation of ϵ

Once the value of the calibration constant is obtained, it is necessary to verify if this value is the correct one to be applied to convert signals in Volts to Watts, or vice-versa. To do this verification, the input power values were calculated based on the heat flow sensors output signals and considering the average calibration constant for each temperature. Based on Figures 3.7a & 3.7b , the conclusion is that the obtained calibration constants work properly since the calculated values of input power were approximately the same as the actual values of input power. That can be verified by the fact that both curves overlap each other for both values of the tested temperatures.
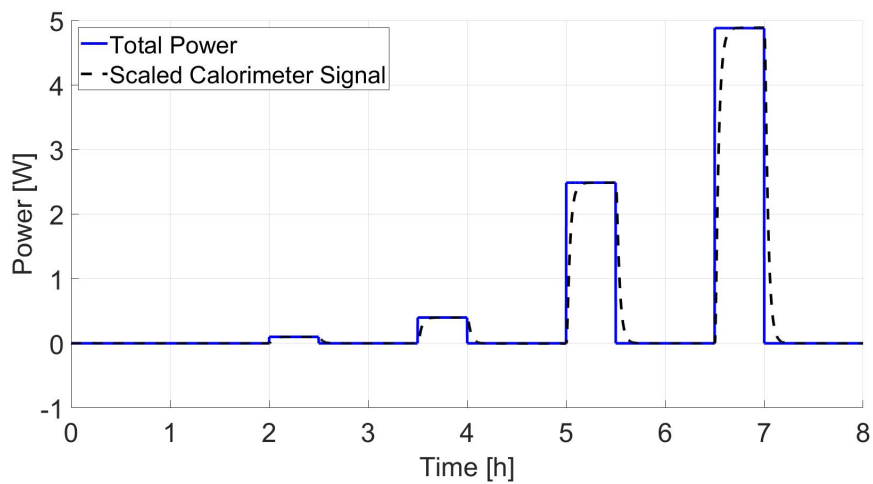
(a) Comparison between measured and calculated power values considering a heat sink temperature of 20°C.
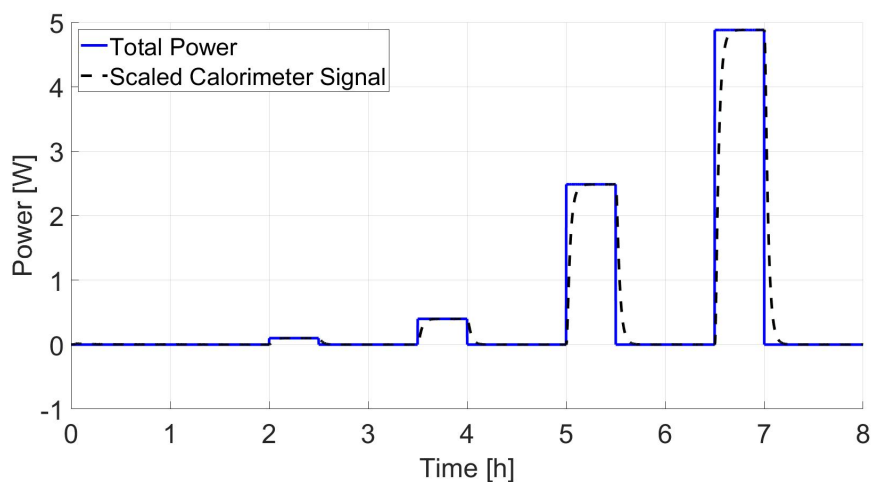
(b) Comparison between measured and calculated power values considering a heat sink temperature of 30°C.

Figure 3.7: Calculated and measured power levels comparison from the calibration procedure.

4

Measurement of specific heat capacity

The method development for the measurement of the specific heat capacity is presented and described in this chapter. All the procedures implemented were based on the absorbed heat measurement concept. Lastly, the validation process of the proposed method is explained, and its results detailed at the end of the chapter.

4.1 Method Development

The method was developed based on some initial assumptions. Firstly, it was considered that the system inside of the calorimeter's box was properly isolated from the outside environment interference. Secondly, the temperature inside the box was considered to remain constant during the entire experiment, providing an isothermal condition. Moreover, the sample's temperature is estimated utilizing the average of the temperature readings from the temperature sensors located in plates SA and SB. Finally, as mentioned before, the main concept for the method development was the absorbed heat measurement.

4.1.1 Absorbed heat concept

For the measurement of the specific heat capacity, the absorbed heat concept was applied to the IHC set-up. This method is based on applying a known temperature step to the calorimeter, controlling the temperature of the water that flows through the heatsinks, and measuring the heat flow output signals from the calorimeter. The set-up configuration for this method was the following: The sample was placed between plates set S, while plates set R, responsible for providing the reference signal, was left empty. The temperature step was applied by controlling the temperature of the water from the heatsinks, and that was done utilizing the Julabo F25MA thermal bath. For all the methods tested in this section, an increasing and decreasing temperature step of the same magnitude was always utilized. The remaining set up details can be found in chapter 3. The complete assembled set up can be seen in Figure 4.1.
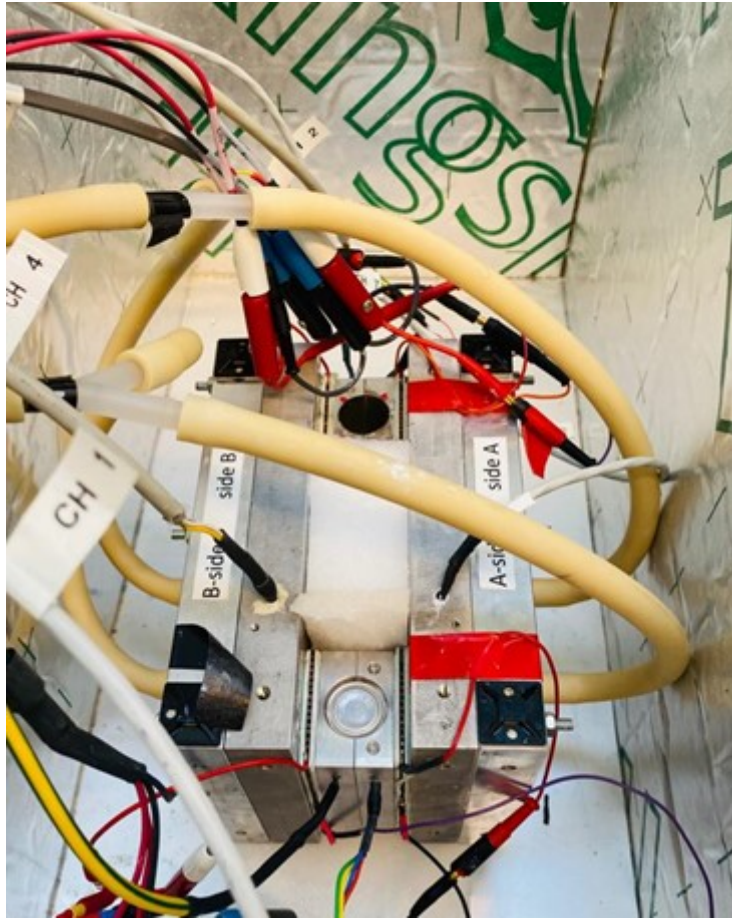
Figure 4.1: Calorimeter set-up for the specific heat capacity measurements.

4.1.2   Temperature step method

In the first approaches, the system was kept at a temperature T_1, in a constant temperature condition, then a temperature increase/decrease step was applied, making the temperature of the system change to T_2. The number of resulting samples depended on the magnitude of the temperature variation step (ΔT) and on the desired temperature range e.g. considering a ΔT of 2°C, and a temperature range from 20°C to 24°C, there would be 4 samples to analyse: 20°C to 22°C, 22°C to 24°C, 24°C to 22°C and 22°C to 20°C (Figure 4.2). The time taken to increase T_1 to T_2, $t_{increase}$, is also an important parameter to consider. The voltage output signals from the heat flow sensors were converted to power signals using the calibration coefficient. After applying the proper offset and bias corrections, the reference signal was utilized to extract the heat flowing only through the sample, called P_{sample}. Finally, P_{sample} was integrated to obtain the total energy absorbed by the sample (E_{sample}). Following the mentioned conditions and procedures, the specific heat capacity could be calculated according to

$$C_p = \frac{E_{sample}}{m \cdot \Delta T} \tag{4.1}$$
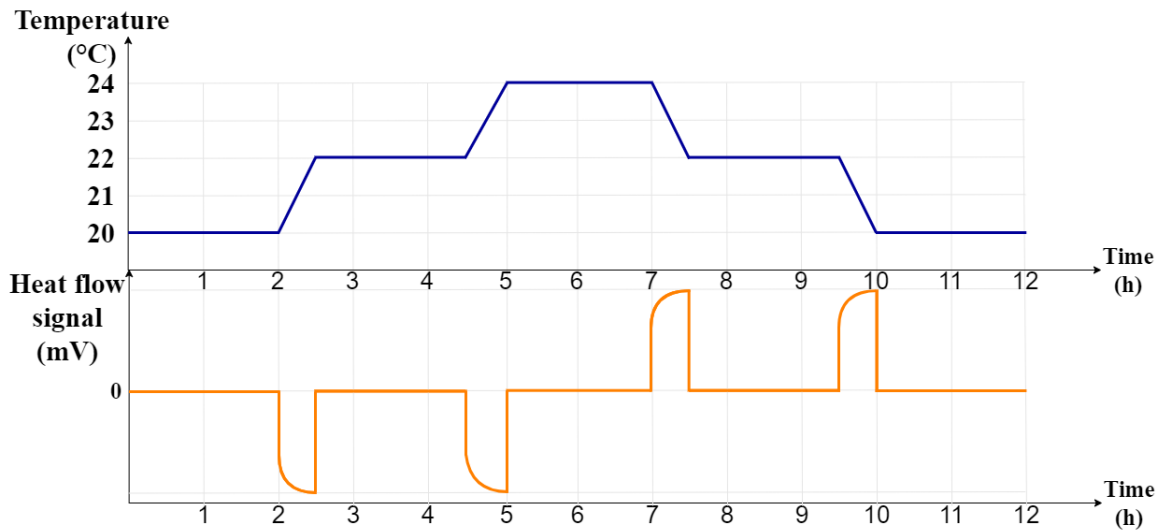
Figure 4.2: Temperature and heat flow signal profiles representation considering ΔT=2°C and a temperature range from 20°C to 24°C.

where E_{sample} is the total energy absorbed by the sample [J], ΔT is the temperature variation [°C], and m is the sample's mass [kg].

As mentioned before, $t_{increase}$ is an important parameter to consider. Since the ideal scenario is to maintain the temperature inside the box as constant as possible, $t_{increase}$ must be long enough to provide a smooth temperature increase for the whole system, in order to avoid undesired temperature differences in certain regions, meaning undesired heat flows, possibly affecting the measurements. Therefore, after considering different values for $t_{increase}$, it was concluded that 30 minutes would be enough to provide such conditions.

After running the first experiments, some issues related to the temperature readings were faced. The already installed heat sinks were not enough to secure the isothermal condition during the temperature increase step, resulting in temperature oscillations inside of the box, which impacted the experiments results. Therefore, in order to solve the temperature oscillations problem, a new heat sink was added to the set-up. The new heat sink was installed as shown in Figure 4.3, where the in channel was connect to the output channel of the previous heat sink, and its output channel was connected to the Julabo F25MA thermal bath. After the installation of the new heat sink, the oscillations of the temperature readings were controlled and the experiments could be continued.

4.1.3 Linear temperature increase method

Another strategy for the temperature variation was also implemented and evaluated. Instead of increasing/decreasing the temperature as described on section 4.1.2, the idea was to increase/decrease 1°C along 1 hour, and not allow the system to rest at
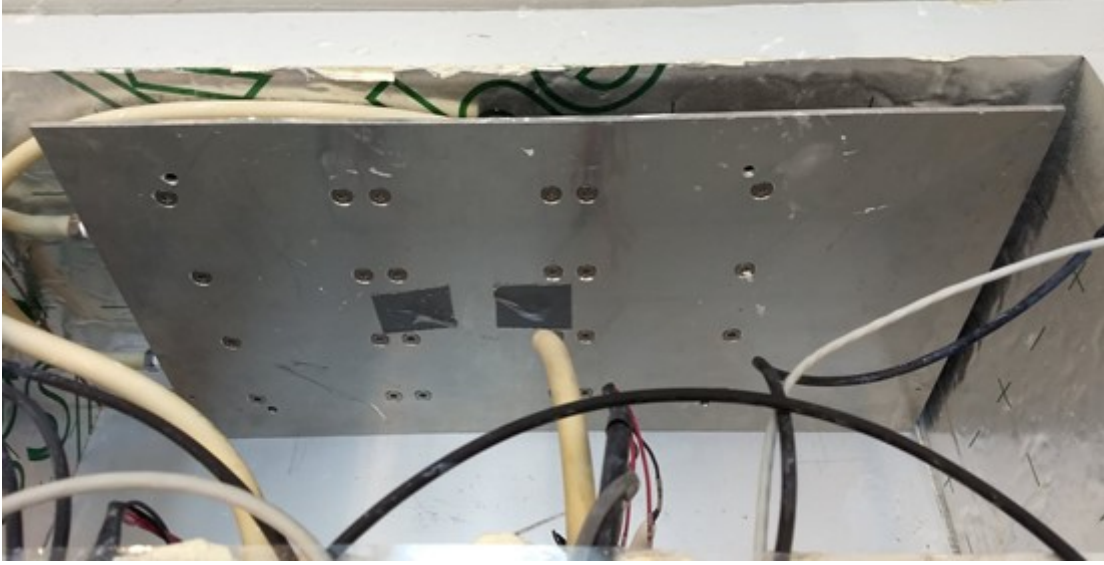
Figure 4.3: Additional heat sink.

a fixed temperature while being at an increasing or decreasing cycle. The mentioned conditions would provide more stability when it comes to the system temperature, since it is composed by a small temperature increase distributed along a long period. This logic is composed by two cycles: In the first one, the temperature is increased 1°C along 1 hour until it reaches the maximum stipulated temperature. The system is then put to rest at a constant temperature for 2 hours, to achieve thermal equilibrium. After the resting period, the second cycle is applied, and the temperature is decreased 1°C per hour until it reaches the lower temperature limit. Figure 4.4 illustrates an example of the temperature and heat flow profiles for this method considering a temperature range from 20°C to 30°C.

The procedure of converting and correcting the signals from the heat flow sensors, mentioned in section 4.1.2, was again performed. However, instead of registering the total energy absorbed by the sample as a voltage signal, E_{sample} was acquired in form of a vector of accumulated values of energy. Another vector with the respective temperature values of the sample (T_{vec}) was also acquired. Furthermore, E_{sample} was plotted as a function of T_{vec}, and a linear function was interpolated (see Figure 4.5). The slope of the interpolated line ($\Delta E_{sample}/\Delta T_{vec}$), which represents [J/°C], was utilized for the calculation of the specific heat capacity, as shown in

$$C_p = \frac{\frac{E_{sample}}{\Delta T_{vec}}}{m} \tag{4.2}$$

where $\Delta E_{sample}/\Delta T_{vec}$ is the slope of the interpolated line [J/°C] and m is the sample's mass [kg].
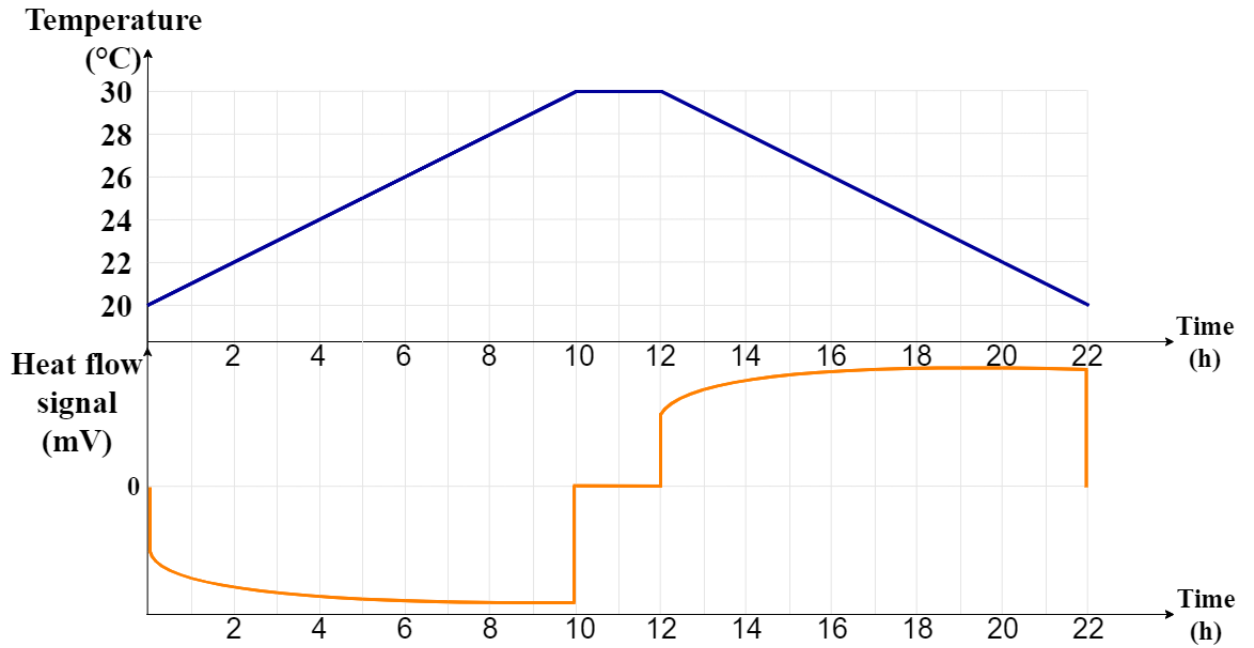
Figure 4.4: Temperature and heat flow signal profiles representation considering temperature range from 20°C to 30°C.
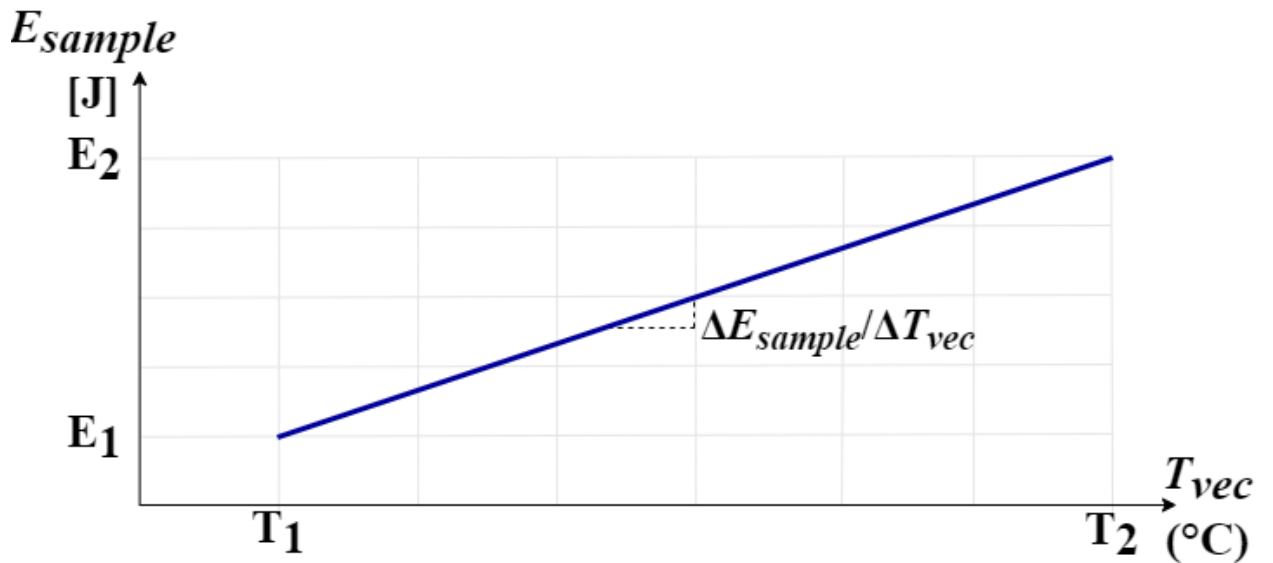
Figure 4.5: E_{sample} vs T_{vec}.

4.2 Validation

For the validation process, a Polyoxymethylene (POM) rod with the same dimensions of a 21700 cylindrical cell was utilized. The measurements were conduct as described in sections 4.1.2 and 4.1.3. The results for the temperature step method, before and after the addition of the new heat sink, are shown in Table 4.1 and Table 4.2. Both experiments were conducted considering ΔT=2°C, and a temperature range from 20°C to 24°C, in order to have a small temperature step, reducing the

heat losses, and stay as close as possible to the ambient temperature (20°C).

Table 4.1: Results from specific heat capacity measurements, temperature step method - 1 heat sink.

Temperature variation	Specific heat capacity [J/kg.°C]	Deviation from the data sheet value (1.50E+03 [J/kg.°C])
20°C to 22°C	1.34E+03	-11%
22°C to 24°C	1.30E+03	-13%
24°C to 22°C	1.47E+03	-2%
22°C to 20°C	1.36E+03	-9%

Table 4.2: Results from specific heat capacity measurements, temperature step method - 2 heat sinks.

Temperature variation	Specific heat capacity [J/kg.°C]	Deviation from the data sheet value (1.50E+03 [J/kg.°C])
20°C to 22°C (1)	1.34E+03	-11%
22°C to 24°C (1)	1.34E+03	-11%
24°C to 22°C (1)	1.51E+03	1%
22°C to 20°C (1)	1.39E+03	-7%
20°C to 22°C (2)	1.39E+03	-7%
22°C to 24°C (2)	1.35E+03	-10%
24°C to 22°C (2)	1.52E+03	1%
22°C to 20°C (2)	1.46E+03	-3%

It can be noted that the Deviation value fluctuates considerably on both conditions. In fact, the new heat sink was added with the intention to make the resulting values more stable, in terms of repeatability. However, even with the addition of the new heat sink, it is noticeable that a fair variation remains. Therefore, the method described in section 4.1.2 was implemented as an attempt to mitigate the mentioned variations. The idea behind the second method is that, by applying a continuous increase of temperature during a long time, the system will have more appropriate conditions to keep a quasi-isothermal environment overall, mitigating any issues related to undesired temperature differences inside the box. The experiment was conducted 5 times, in order to evaluate the repeatability of the method, considering a temperature range from 18°C to 22°C. The results for this method can be seen in Table 4.3.

By analysing the results, it is possible to see that, besides some few exceptions, the Deviation value oscillated little, and it is inside of a reasonable range of Deviation (less or equal to 10% in all cases). Figure 4.6 shows the experiment's temperature profile, and Figure 4.7 shows the corrected signals from the heat flow sensors attached to plates SA and SB, which represents the amount of heat being transferred only to the cell. It is possible to see that the voltage magnitude from the signals

Table 4.3: Results from specific heat capacity measurements, linear increase method - 2 heat sinks.

Temperature variation	Specific heat capacity [J/kg.°C]	Deviation from the data sheet value (1.50E+03 [J/kg.°C])
18°C to 22°C (1)	1.51E+03	1%
22°C to 18°C (1)	1.36E+03	-9%
18°C to 22°C (2)	1.43E+03	-5%
22°C to 18°C (2)	1.35E+03	-10%
18°C to 22°C (3)	1.41E+03	-6%
22°C to 18°C (3)	1.39E+03	-7%
18°C to 22°C (4)	1.39E+03	-7%
22°C to 18°C (4)	1.40E+03	-7%
18°C to 22°C (5)	1.38E+03	-8%
22°C to 18°C (5)	1.39E+03	-7%

presented a considerably low value, less than 0.6 [mV]. A similar scenario was identified in the previous method, where the magnitude of the signals was around 2 [mV]. Such a low magnitude could contribute to errors related to the measurement equipment, since there is a huge dependency on the sensors resolution limits in order to identify the small difference between the total heat being transferred to the whole calorimeter, and the amount of heat being transferred only to the sample. At last, considering all the acquired results, the linear increase method was chosen to be applied in the cell's measurements.
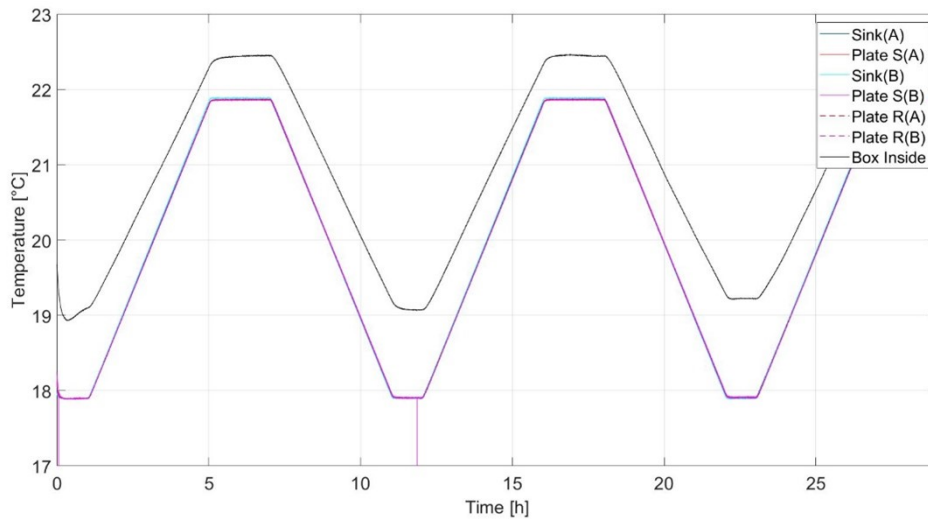
Figure 4.6: Temperature profile from the first 3 cycles of experimental application of linear increase method.
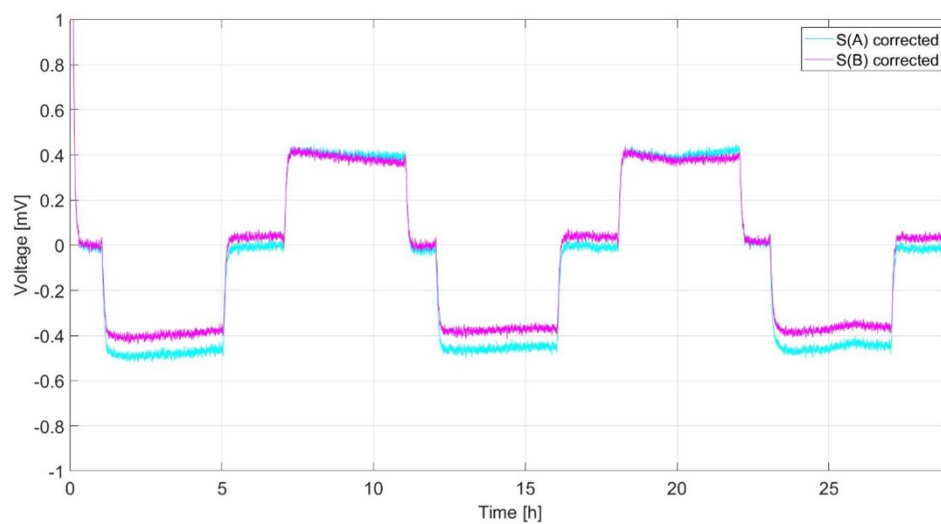
Figure 4.7: Corrected SA and SB signals from the first 3 cycles of experimental application of linear increase method.

5

Measurement of axial thermal conductivity

The method development for the measurement of the axial thermal conductivity is presented and described in this chapter. The same initial assumptions as mentioned in chapter 4 were considered. The validation process is also presented, followed by the measurement results and some considerations about the experiments.

5.1 Method development

Two relevant directions must be considered when studying the thermal conductivity of a cylindrical cell: the axial direction and the radial direction. Although a third direction does exist, known as the spherical direction, it will not be considered into further analysis. This approach is possible due to the fact that the cylindrical cell has a high number of winds, which results in the heat flow being predominant in the radial direction, even if there is a big difference between the thermal conductivities [18].

For the measurement of the axial thermal conductivity, the same calorimeter set-up used for the measurement of the specific heat capacity was utilized. Additionally, a certain sample's length, called Δx, was placed out of plates set "S". Moreover, a customized heater, described in section 5.1.2, was placed at the top of the sample. The purpose of the mentioned changes was to create a temperature difference along the sample's axial direction. Also, this logic was implemented considering that the pressure plates would be able to maintain the temperature in the remaining sample's length constant, at the same temperature as the heat sinks. Therefore, the temperature at Δx could be acquired by the measurements from the temperature sensors placed inside of pressure plates SA and SB. The temperature from the top of the sample was measured by a modified temperature sensor, described in details in Section 5.1.1. Considering the described experimental set-up, the heat would flow through the sample, and through the plates, until it reaches the heat flow sensors placed between the plates and the heat sinks. The experiment was conducted in cycles, each cycle consisting of 1.5 hours with the heater turned on and 1 hour with the heater turned off (resting period). Figure 5.1 presents a conceptual scheme of the described set-up.
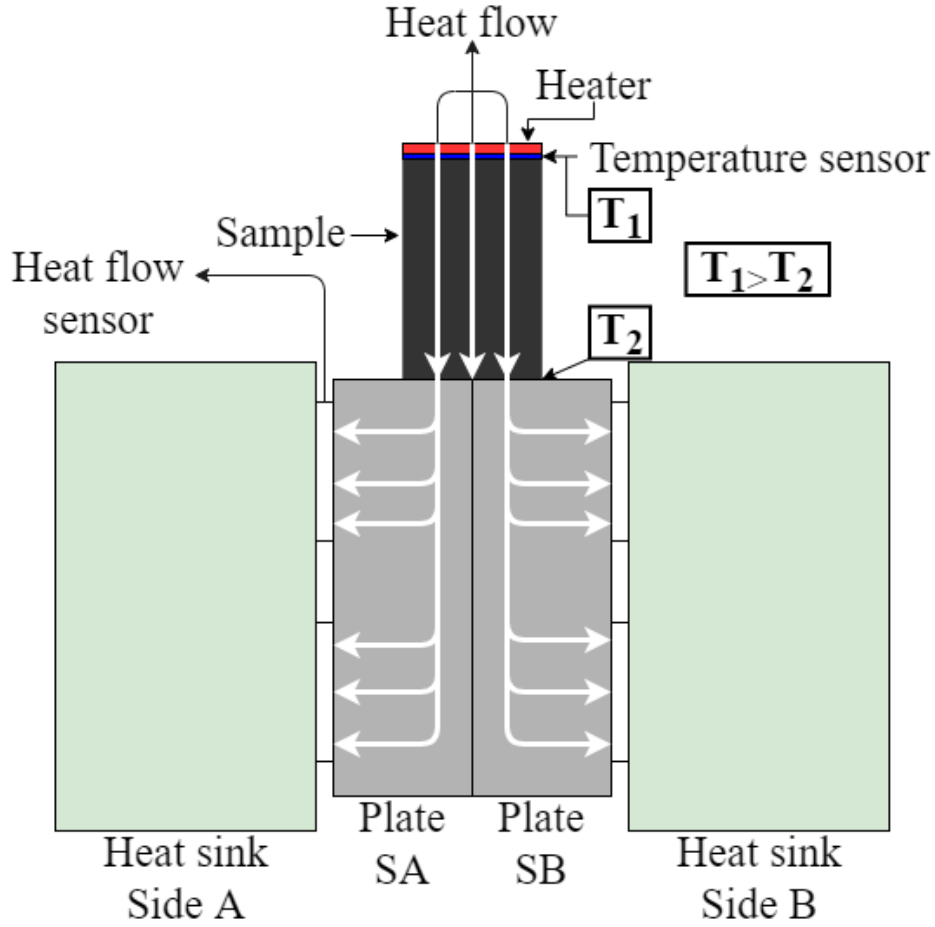
Figure 5.1: Conceptual scheme of the initial measurement strategy.

Assuming a steady state condition, and constant heat flow, the expression to calculate the heat flow only in the axial direction can be derived from (2.3). The one-dimensional steady state heat conduction equation, considering the axial direction, is then obtained as

$$q_{axial} = -K_{axial} \cdot A_{axial} \cdot \frac{\Delta T}{\Delta x} \tag{5.1}$$

where, q_{axial} is the heat flow in the axial direction [W], K_{axial} is the axial thermal conductivity [W/(m.K)], A_{axial} is the cross-section area to the heat flow [m²], ΔT is the temperature difference between T_1 and T_2, and Δx is the sample's length left outside plates set "S" [m]. Solving for K_{axial}, the expression to calculate the thermal conductivity is obtained

$$K_{axial} = \left| \frac{q_{axial}}{A_{axial} \cdot \frac{\Delta T}{\Delta x}} \right| \tag{5.2}$$

Lastly, A_{axial} can be calculated as

$$A_{axial} = \pi \cdot r_{sample}^2 \tag{5.3}$$

where r_{sample} is the sample's radius [m²].

5.1.1 Sample's top temperature sensor

One important aspect to consider is that the temperature sensor placed on the sample's top must have a good contact with the entire sample's top surface, leaving as few gaps as possible. In order to do so, a new temperature sensor was built specially for the experiment's configuration. A square 21x21 mm aluminium plate, 1 [mm] thick, with a small rectangular section on the side, was attached to a PT100 temperature sensor, and the set was covered with an isolation material. The temperature sensor was place on the rectangular section, and cable ties were used to hold the configuration together. This modified temperature sensor was placed between the heater and the sample's top during the experiments. Therefore, thermal pads were added on both surfaces of the square section of the aluminium plate, aiming to improve the thermal contact between the sensor and both the sample's top and the heater. The complete assembled temperature sensor can be seen in Figure 5.2.
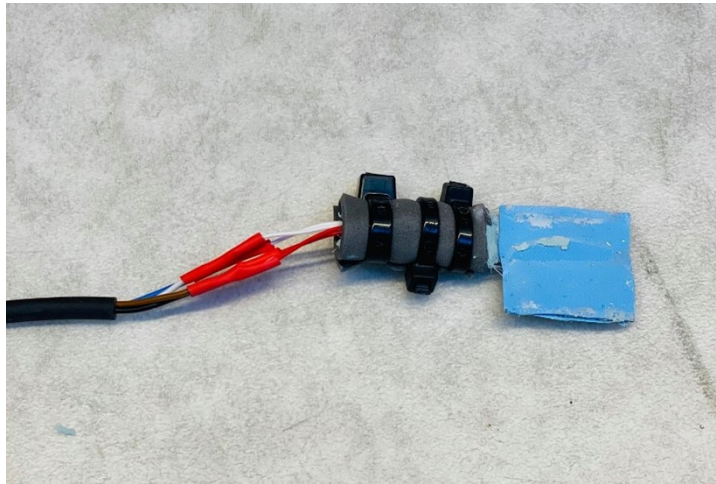
Figure 5.2: Modified temperature sensor applied in the axial thermal conductivity measurements.

As it possible to see from (5.2), even a small deviation in the value of Δx will have a considerable impact on the value of K_{axial}, when it comes to precision. In other words, if there is a deviation of 10% in the value of Δx, it will result in a deviation of 10% in the value of K_{axial}, which is already a significant value in terms of measurements precision. Therefore, considering that the value of Δx is in the order of mm, it is very important that the distance from the temperature sensor to the cell's top be measured with suitable equipment, in order to secure a good precision.

5.1.2 Customized experimental heaters

The heater is a fundamental part in the experimental set-up since it is the responsible for providing the temperature difference in the system. Two different heater configurations were tested. The first one was a heater composed by three 110 [Ω], (12 [V]/1.25 [W]), resistors connected in series, totalizing a maximum power of 3.75 [W]. The heater is shown in Figure 5.3. Later, another heater was built, composed

by a single 3 [W], 47.5 [Ω], resistor. As it is possible to see in Figure 5.4, the second heater is considerably smaller than the first one. Therefore, the purpose of utilizing the second heater was to provide a more optimized heat distribution in the sample's top, as well as reducing the heat losses.

Figure 5.3: First heater utilized in the axial thermal conductivity experiments.

Figure 5.4: Second heater utilized in the axial thermal conductivity experiments.

5.2 Validation

For the validation process, a Polyoxymethylene (POM) rod with the same dimensions of a 21700 cylindrical cell was utilized. The measurements were conducted considering the experimental set-up described in section 5.1. Two different configurations were applied in the validation process:

- Configuration 1: First heater, $\Delta x = 35$mm.
- Configuration 2: Second heater, $\Delta x = 10.5$mm.

Figure 5.5 and Figure 5.6 show the complete assembled set up for both configurations. The experimental results, as well as the power applied to the heater, can be seen in Table 5.1 and Table 5.2.
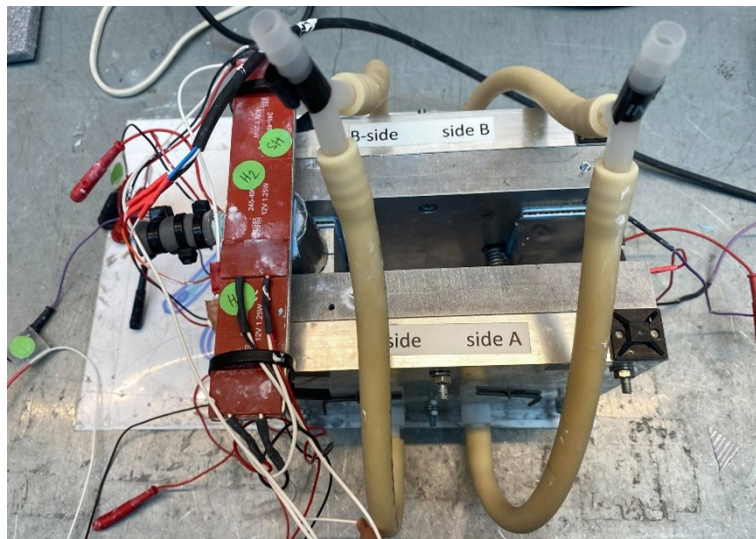
Figure 5.5: Experimental set-up - Configuration 1.
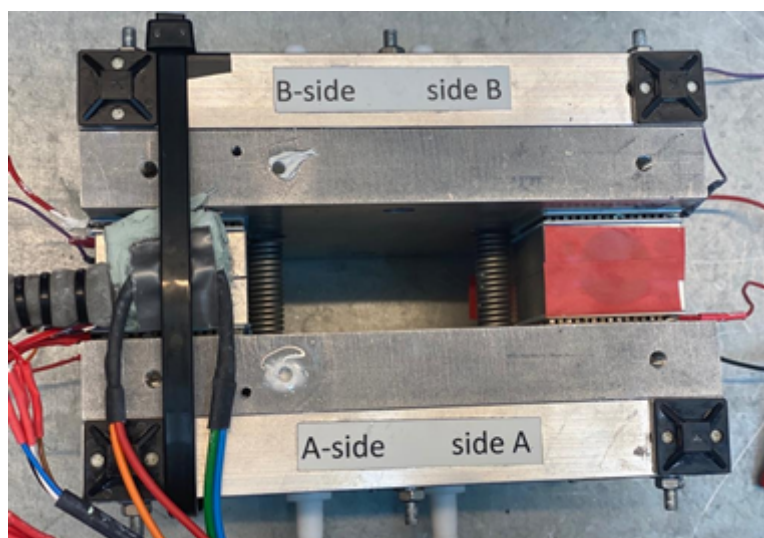
Figure 5.6: Experimental set-up - Configuration 2.

Table 5.1: Measurements results for configuration 1.

Heat power	Measured power	Measured/input power ratio	Ka [W/m.K]	Deviation from the data sheet value (0.31[W/m.K])	ΔT [°C]
0.30	0.005	2%	0.1653	-47%	3.36
0.44	0.0086	2%	0.2022	-35%	4.29
1.11	0.0221	2%	0.2351	-24%	9.51
1.38	0.0196	1%	0.2324	-25%	8.5386
1.76	0.03	2%	0.2258	-27%	13.77

Table 5.2: Measurements results for configuration 2.

Heat power	Measured power	Measured/input power ratio	Ka [W/m.K]	Deviation from the data sheet value (0.31[W/m.K])	ΔT [°C]
0.096	0.0261	27%	0.3613	17%	2.14
0.105	0.0247	24%	0.324	5%	2.31
0.109	0.0239	22%	0.3186	3%	2.27
0.119	0.0286	24%	0.3486	12%	2.44
0.128	0.0286	22%	0.3348	8%	2.59
0.133	0.0304	23%	0.3429	11%	2.68
0.144	0.0377	26%	0.3774	22%	2.97
0.171	0.0449	26%	0.3866	25%	3.45
0.201	0.0469	23%	0.3696	19%	3.84
0.267	0.062	23%	0.3797	22%	4.95

Regarding configuration 1 results, some points must be highlighted. Firstly, the power ratio between the applied power to the heater and the actual heat being transferred to the sample presented very low values (no greater than 2%). This can be associated with the fact that the first heater utilized had a large area that was not is contact with the top of the cell, which could significantly increase the power losses. Secondly, to avoid even more power losses, ΔT was meant to stay in a range from 2°C to 4°C, however the heat flow readings considering the mentioned temperature range were quite low, resulting in unreadable measurements or results with low consistency. Lastly, the obtained values of K_a were considerably far from the data sheet value, besides the fact that a good consistency was only achieved when working with high values of ΔT (above 9°C). Therefore, configuration 2 was implemented, utilizing a smaller heater, and reducing Δx to make the power losses lower.

Analysing the results from configuration 2, it becomes clear that 3 main improvements were achieved. First, the power ratio increased significantly, which can be an indicative that utilizing a smaller heater, better fitted to the top of the cell, as well as decreasing Δx, helped to avoid power losses. Second, it was possible to run the experiments for values of ΔT inside of the stipulated range, possibly due to

the fact that the power ratio was improved, decreasing the necessary heater input power, which could be contributing for higher temperature readings since the heater is attached to the temperature sensor's plate. Third, the values obtained for K_a presented a far better consistency, and the Deviation from the data sheet value was also substantially reduced. Thus, configuration 2 was chosen to be applied in the cell's measurements.

6

Measurement of radial thermal conductivity

This chapter describes the method development for the last cell's thermal parameter covered in this thesis: The radial thermal conductivity. Once again, the same initial assumptions mentioned in Chapter 4 and Chapter 5 were considered. The validation process is presented at the end of the chapter, also including measurement results and relevant comments on the experimental process.

6.1   Method development

Together with the specific heat capacity and the axial thermal conductivity, the radial thermal conductivity completes the basic set of thermal parameters necessary to carry out studies on thermal characterization of cylindrical Li-ion battery cells. To perform the measurements, a certain path was chosen considering the radial direction, considering two points: The cell's surface and Δx mm away from it. Furthermore, the distance between the two points needed to be measured with suitable measurement equipment, which had a good precision at the mm level, and the temperature at the two points needed to be known. Lastly, it was also necessary to establish a heat flow only through the sample's radial direction.

Thus, a 3 mm thick hole was drilled through the sample's centre, and a 2.5 mm thick hole was drilled at Δx mm from the sample's surface. The hole in the centre passed through the entire sample, and the other one was 5mm deep. A custom-made heater, described in Section 6.1.1, was placed in the first hole, and a PT100 temperature sensor was placed in the second one. Then, the sample was placed entirely between plates set "S", so the temperature at the sample's surface would remain constant (controlled by the heat sinks temperature). Therefore, the heater was responsible for providing the heat flow through the radial direction, since the sample's surface and centre temperatures could be considered as constant, and the additional temperature sensor would record the temperature from Δx mm from the sample's surface. Similar to what was done for the axial thermal conductivity measurements, the experiments were conduct in cycles, each cycle composed by 2 hours of heater on and 2 hours of heater off (resting period). Figure 6.1 shows a conceptual scheme from the experimental set-up, and Figure 6.2 shows a picture from the utilized POM sample.

Assuming a constant heat flow in the radial direction, and that the system is operating in a steady state condition, the equation to calculate the heat flowing through the radial direction can be obtained from (2.2). The result is the one-dimensional steady state heat conduction equation for the radial direction

$$q_{radial} = \frac{-2 \cdot \pi \cdot K_{radial} \cdot l_{sample} \cdot \Delta T}{\ln\left(\frac{r_{sample}}{r_{sample} - \Delta x}\right)} \tag{6.1}$$

where, q_{radial} is the heat flow in the radial direction [W], K_{radial} is the radial thermal conductivity [W/(m.K)], l_{sample} is the samples's length [m], ΔT [K] is the temperature difference between Δx mm from the sample's surface (T_1) and the sample's surface (T_2), Δx is distance between the temperature sensor and the sample's surface [m], and r_{sample} is the sample's radius. Therefore, K_{radial} can be calculated as

$$K_{radial} = \left| -\frac{q_{radial} \cdot \ln\left(\frac{r_{sample}}{r_{sample} - \Delta x}\right)}{2 \cdot \pi \cdot l_{sample} \cdot \Delta T} \right| \tag{6.2}$$
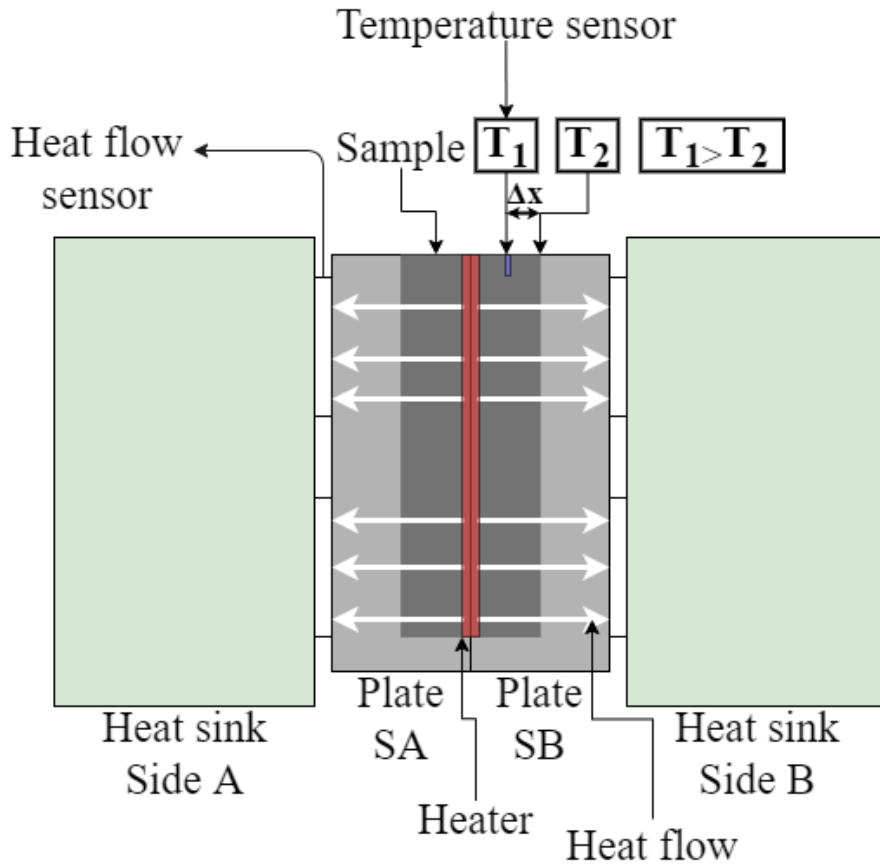
Figure 6.1: Conceptual scheme from the experimental set-up for the radial thermal conductivity measurements.

Figure 6.2: POM sample utilized in the validation process.

6.1.1 Custom-made heater

The heater utilized in the radial thermal conductivity measurements were composed by 3 resistors of 1 [W] connected in series, totalizing a maximum power of 3 [W], with a measured resistance of 8.3 [Ω]. The mentioned heater is presented in 6.3.
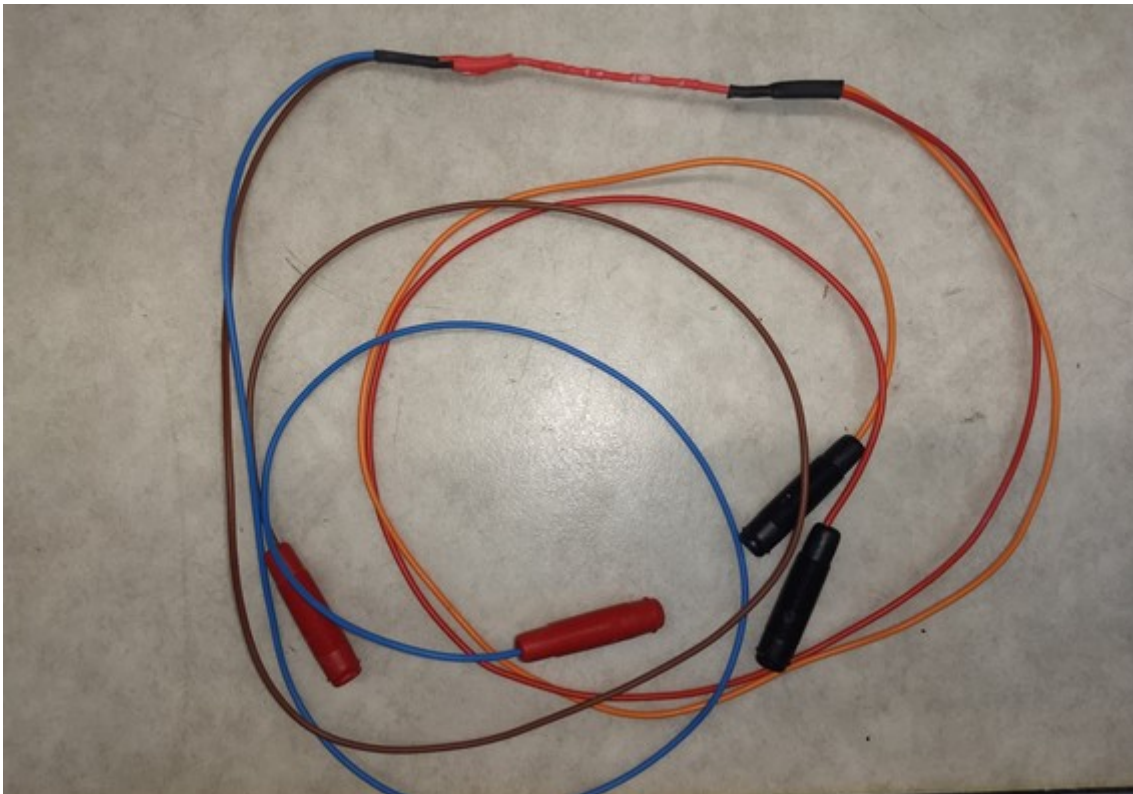
Figure 6.3: Custom made heater utilized in the validation process.

6.2 Validation

The validation process was conducted utilizing a Polyoxymethylene (POM) rod with the same dimensions of a 21700 cylindrical cell. The experiments were performed according to the method described in section 6.1, considering $\Delta x = 4.5$mm. The used set-up is shown in Figure 6.4, and the experimental results are presented in Table 6.1.
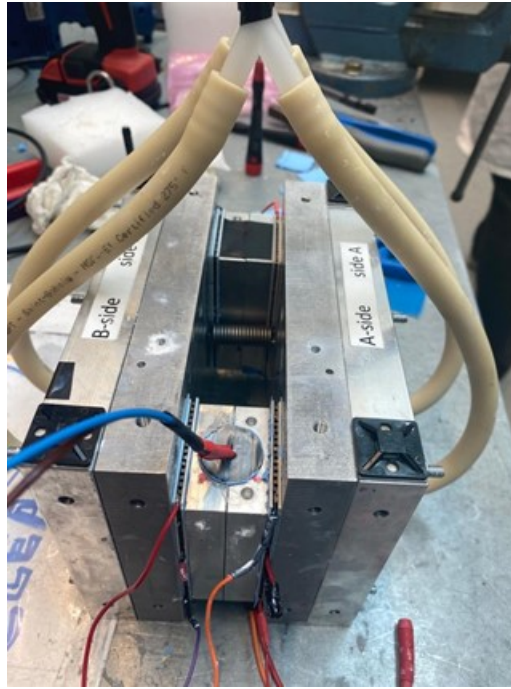
Figure 6.4: Calorimeter set up for the radial thermal conductivity measurements.

Table 6.1: Experimental results for the radial thermal conductivity measurements.

Heat power	Measured power	Measured/input power ratio	Kr [W/m.K]	Deviation from the data sheet value (0.31[W/m.K])	ΔT [°C]
0.332	0.267	81%	0.341	10%	1.02
0.401	0.339	84%	0.345	12%	1.28
0.518	0.424	82%	0.344	11%	1.61
0.605	0.515	85%	0.341	10%	1.98
0.747	0.602	81%	0.334	8%	2.37
0.849	0.720	85%	0.347	12%	2.71
0.959	0.783	82%	0.354	14%	2.89
1.016	0.833	82%	0.341	10%	3.19

Analysing the results, it is possible to see that the power ration between the applied power to the heater and the actual heat being transferred to the sample presented good values, being greater than 80%. Regarding the temperature variation, the intention was to keep its value inside of range from 1°C to 3°C, since high values of temperature variation could contribute to increase the heat losses, and, as it is possible to verify in Table 6.1, this measurements were successfully performed for the mentioned range. Moreover, the values of K_r presented a great consistency, and good Deviation values in general (below 15%). Therefore, the described method was considered suitable for application in the cell measurements.

7
Results and analysis

The results and analysis of the thermal properties measurements of the cylindrical Li ion battery cell are presented in this chapter. A full description of the cell utilized in the measurements can be found in Table 7.1, and a picture of the cell can be found in Figure 7.1.

Table 7.1: Cylindrical cell's technical description.

Cell model	Voltage operation range [V]	Capacity [Ah]	Dimensions [R x L] mm	Weight [g]	Chemistry
TESLA 21700 cylindrical cell	2.5 - 4.2	4.5	21x70	69	NCA

Figure 7.1: Tesla cell utilized in the measurements.

7.1 Specific heat capacity (C_p)

The measurements of the specific heat capacity were performed as described in Chapter 4, considering a temperature range from 18°C to 22°C. The obtained specific heat capacity value, together with the respectively measurement variation, are presented in Table 7.2. The resulting value of C_p can be considered as a reasonable one, since it is close to already reported specific heat capacity values for cylindrical Li ion cells, found in the literature [19], [20]. The measurement variation also presented a good result, showing a fair level of variation. At last, the acquired experimental data of heat flow and temperature variation, utilized for the cell's C_p calculation, are presented in Figure 7.2 and Figure 7.3.

Table 7.2: Specific heat capacity of the 21700 NCA cylindrical Li ion cell.

Measured Value [J/kg.°C]	Measurement variation [J/kg.°C]
841	±27.1
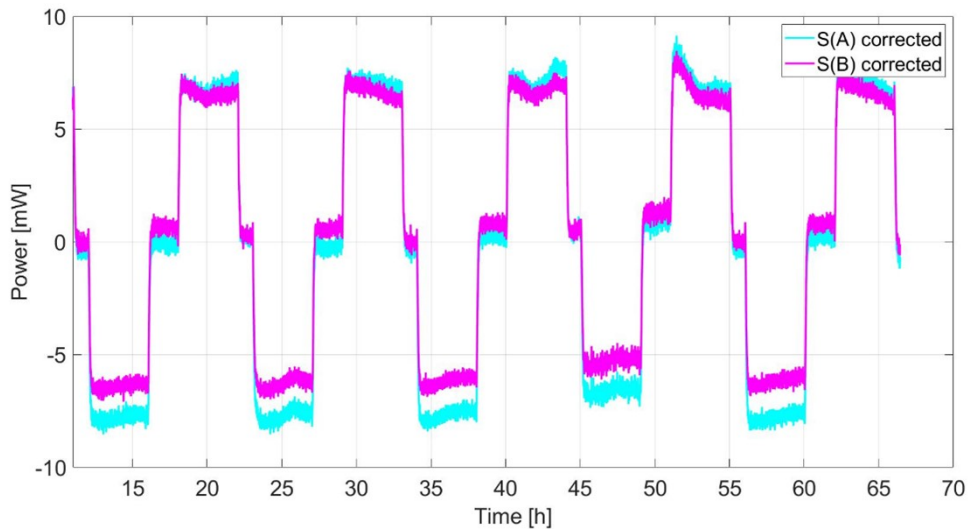
Figure 7.2: Corrected heat flow signals utilized for the cell's Cp determination.

7.2 Axial thermal conductivity (K_a)

The measurements of the cell's axial thermal conductivity were performed according to the method described in Chapter 5 (axial thermal conductivity chapter). As it can be seen in Table 7.3, the acquired cell's (K_a value is 6.93 ± 0.1 [W/m.K], which is considerably below the expected axial thermal conductivity value for cylindrical Li ion cells. Therefore, some modifications were implemented to the original method mentioned in Chapter 5. An extra PT100 temperature sensor was attached to the cells surface, as shown in Figure 7.4, in order to avoid wrong temperature
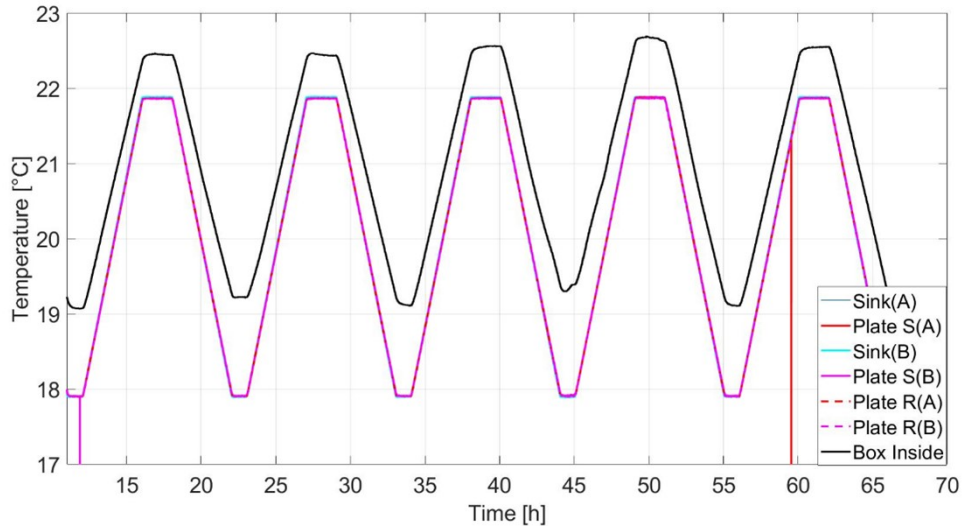
Figure 7.3: Temperature signals utilized for the cell's Cp determination.

measurements resulted from the existing close contact between the heater and the modified temperature sensor. Moreover, a new parameter Δx_2 was defined, being the distance from the new temperature sensor to the plates set "S". Regarding K_a calculations, the path considered for the calculations needed to be changed, in order to fit the modified experimental set-up. Therefore, the new path considered the distance between the new temperature sensor to the plates set "S". Furthermore, instead of using Δx in 5.2, Δx_2 was the utilized distance, and the variation of temperature was considered between the new temperature sensor and the average of the temperature readings from plates SA and SB. At last, a new test was performed based on the mentioned modifications and considering $\Delta x_2 = 10$mm. The results are presented in Table 7.4.

Table 7.3: Acquired axial thermal conductivity of the 21700 NCA cylindrical Li ion cell without the extra temperature sensor.

Measured Value [W/m.K]	Measurement variation [W/m.K]
6.93	±0.1

Table 7.4: Axial thermal conductivity value of the 21700 NCA cylindrical Li ion cell considering the extra temperature sensor.

Measured Value [W/m.K]	Measurement variation [W/m.K]
11.55	±0.1

The result acquired from the modified method is more in agreement with the expected result for a cylindrical Li ion battery cell, moreover, the measurement variation also presented a good result, confirming the consistence of the presented

Figure 7.4: Additional temperature sensor attached to the cell's surface.

method. Lastly, Figure 7.5 and Figure 7.6 show 3 of the temperature and corrected heat flow samples utilized for the determination of K_a.
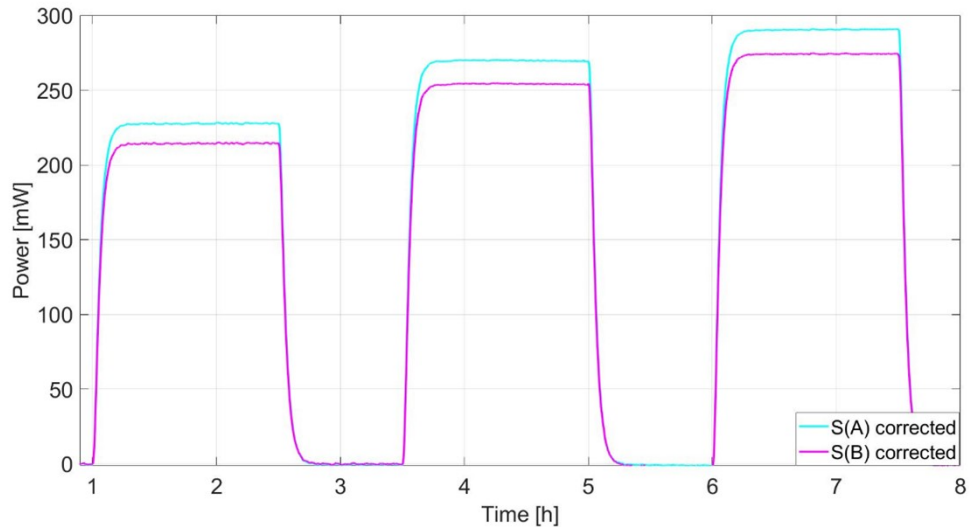
Figure 7.5: 3 Samples of the corrected heat flow signals from the cell's axial thermal conductivity measurements.
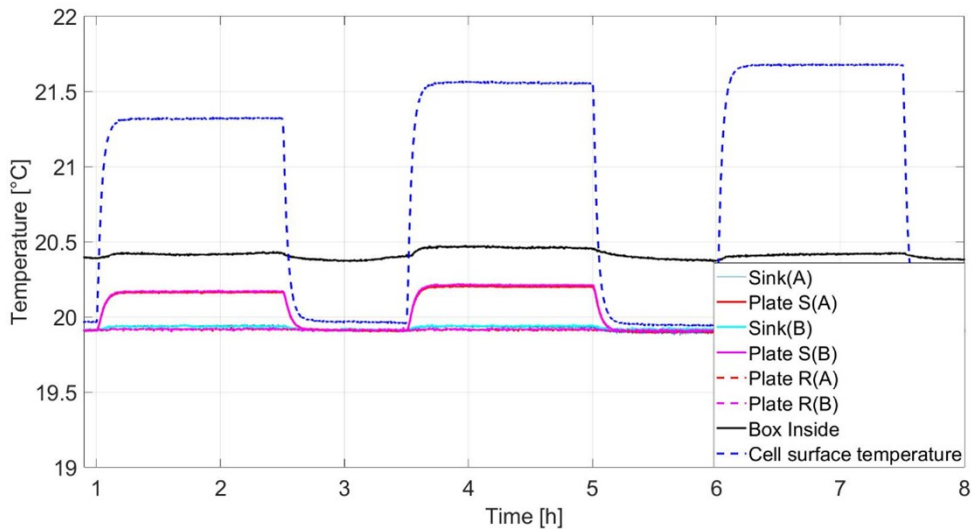
Figure 7.6: 3 Samples of the temperature signals from the cell's axial thermal conductivity measurements.

7.3 Radial thermal conductivity (K_r)

The method utilized for the measurements of the radial thermal conductivity of the cylindrical Li ion cell is described in Chapter 6. However, due to technical issues, the heater utilized for the experiments needed to be modified in order to better fit the cell's design. The new heater was composed by 2 resistors of 3 [W] connected in series, with a total measured resistance of 95 [Ω], attached to a cooper rod. The cooper rod was placed inside of the hole drilled in the cell's centre. Additionally, another change made was that the hole drilled in the cell's centre did not pass through the entire cell, having a total depth of 35mm instead. Before the drilling process be performed, due to safety reasons, the cell was completely discharged with a C/10 rate, and short circuited for 1 week, so the cell could be considered electrical inactive. Once the hole for the heater and the temperature sensor were drilled, they were immediately filled up with the X60 cold curing glue [30], produced by HBM, responsible for both filling up the gap left by the drilling, avoiding electrolyte leakage, and also for fixation. Figure 7.7 shows an image from the utilized heater, and Figure 7.8 shows an image from the cell with both the temperature sensor and the heater already installed. Furthermore, the obtained value of the radial thermal conductivity is shown in Table 7.5.

Table 7.5: Radial thermal conductivity value of the 21700 NCA cylindrical Li ion cell considering.

Measured Value [W/m.K]	Measurement variation [W/m.K]
0.83	±0.04

Both temperature and heat flow signals were satisfactorily stable during the measurements. In addition to that, the resulting value of the cell's radial thermal con-

Figure 7.7: Heater utilized in the measurements of the cell's radial thermal conductivity.

Figure 7.8: Drilled cell both the temperature sensor and the heater installed.

ductivity presented a very good consistency, as it is possible to see from the value of the measurement variation. Finally, Figure 7.9 and Figure 7.10 show 3 of the corrected heat flow and temperature samples utilized for the determination of K_r.
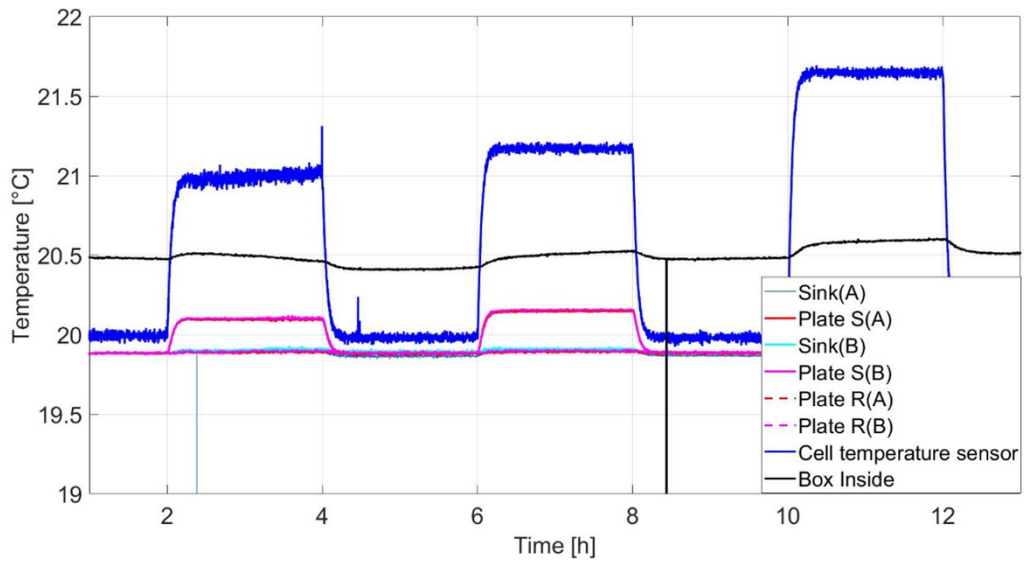
Figure 7.9: 3 Samples of the temperature signals from the cell's radial thermal conductivity measurements.
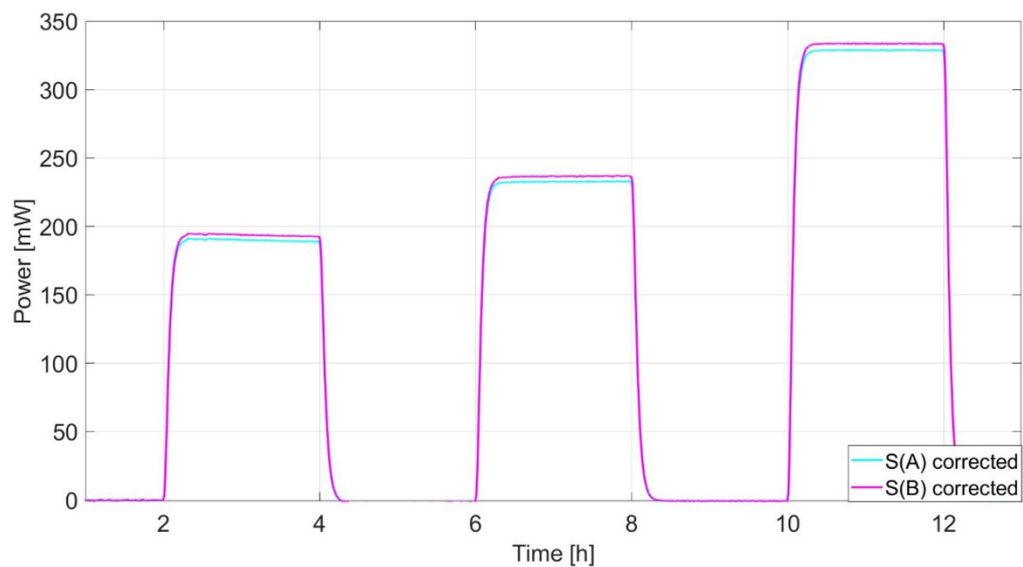
Figure 7.10: 3 Samples of the corrected heat flow signals from the cell's radial thermal conductivity measurements.

8
Conclusion

The main focus of this master thesis work was to modify and improve a custom-made Isothermal Heat Conduction (IHC) calorimeter, designed to operate with prismatic and pouch Li ion cells, in order to be applied in thermal characterization of cylindrical Li ion cells. Considering the results obtained, the modifications were successful, and it was proved that the calorimeter is well suitable for the designed task.

Some issues related to heat leakage were faced when the measurements of specific heat capacity were performed, highlighting the importance of having an isothermal environment condition secured during the entire test, especially when performing tests that involve considerably low heat flow signals to be measured. It was noted that even small variations in the temperature outside of the isolation box were interfering with the measurements. The issues were overcome by adding a new heat sink to the calorimeter set-up, and applying the linear temperature increase method, in order to keep the temperature inside of the box as constant as possible. The measured Cp value of the cylindrical Li ion cell was 841 [J/kg.°C].

The axial thermal conductivity was measured for different power levels, respecting a maximum temperature variation range around 3ºC. After applying a better designed heater in the set-up, the resulting measurements from the validation process presented a really good level of consistency. Regarding the cell's measurements, the position of the temperature sensor, as well as the length of the cell left outside of the calorimeter plates, had to be changed, in order to improve the method's reliability. The main concern was that the temperature sensor and the heater were too close to each other, probably impacting the temperature measurement from the top of the cell. Once the modifications were applied, the measurements presented a good consistency, and the measured cell's axial thermal conductivity was 11.55 [W/m.K].

The method for the measurement of the radial thermal conductivity was also validated for different levels of power, respecting 3°C as maximum temperature variation range. In the validation process, the measurements precision was consistence, presenting good results. For the cell's measurements, the heater needed to be changed to improve its fitting in the cell's centre drilled hole. The strategy of drilling the holes in the cell was successfully applied, having almost no lost of electrolyte. The measured value of the cylindrical cell radial thermal conductivity was 0.83 [W/m.K], presenting a really good precision.

As expected, the axial thermal conductivity of the cylindrical cell is considerably higher than the radial one, due to the fact that in the radial direction, the heat must flow through several layers of materials (cell's active materials, separator, etc), and some of these materials are poor heat conductors, while in the axial direction, the heat will mainly flow through the materials that have the highest thermal conductivities (Aluminium or Copper).

This thesis work presented methods that can be used for the thermal characterization of cylindrical Li ion cells utilizing an IHC calorimeter. The obtained results showed a very good precision, and can be considered has a valuable contribution for thermal management of Li-ion battery packs, since the presented thermal parameters can be applied into further studies, helping to improve the battery management system as whole.

8.1   Future work

Future investigations are necessary to validate the kinds of conclusions that can be drawn from this study. There are quite a few areas in this thesis work that can be improved in the future. For more accuracy of the measurements or improvement of the method below suggestions can be implemented in the future.

- Though having a styrofoam box as insulation for the setup, the inside box temperature was affected by the room temperature. Therefore, the setup can be used inside a new styrofoam box or temperature chamber for getting a consistent temperature around the setup. On the other hand, instead of one cooling plate inside the box, more coolings palates can be used for getting stable temperature around the setup.
- Modified IHC made for only two samples, one more pair of pressure plates (for one sample) can be added in calorimeter for having more accurate measurements.
- The result can be validated by simulation which could be done in Comsol Multiphysics. In order to achieve a more desirable result for designing a cooling system model should more be constructed. As well, the model could be coupled with an electrical model.
- In Future work should consider the potential effects of the low power ratio between the applied power from the heater and actual heat being transferred to the sample in Ka (axial thermal conductivity measurement method). More improved/modified heater could be used to utilize maximum power from the heater to the sample.
- For more understanding of the behavior and the cell, the dependency of thermal properties on temperature, cell SOC and SOH can be further studied.

Bibliography

[1] T. L. Bergman, A. S. Lavine, F. P. Incropera and D. P. Dewitt, *Fundamentals of heat and mass transfer*, 7th *edition*, 2011.

[2] A. Lidbeck and K. R. Syed, "Experimental Characterization of Li-ion Battery cells for Thermal Management in Heavy Duty Hybrid Applications", *Department of Energy and Environment − Division of Electric Power Engineering, CHALMERS university of technology*, 2017.

[3] C. Zhao, W. Cao, T. Dong and F. Jiang, "Thermal behavior study of discharging/charging cylindrical lithium-ion battery module cooled by channeled liquid flow", *International Journal of Heat and Mass Transfer*, vol. 120, pp 751–762, 2018.

[4] W. Cao, C. Zhao, Y. Wang, T. Dong and F. Jiang, "Thermal modeling of full-size-scale cylindrical battery pack cooled by channeled liquid flow", *International Journal of Heat and Mass Transfer*, vol. 138, pp 1178–1187, 2019.

[5] B. Ng, P. T. Coman, W. E. Mustain and R. E. White, "Non-destructive parameter extraction for a reduced order lumped electrochemical-thermal model for simulating Li-ion full-cells", *Journal of Power Sources*, vol. 445, 227296, 2020.

[6] S. Wang, K. Li, Y. Tian, J. Wang, Y. Wu and S. Ji, "An experimental and numerical examination on the thermal inertia of a cylindrical lithium-ion power battery", *Applied Thermal Engineering*, vol. 154, pp 676–685, 2019.

[7] D. Stephens, P. Shawcross, G. Stout, E. Sullivan, J. Saunders, S. Risser, and J. Sayre, "Lithium-ion battery safety issues for electric and plug-in hybrid vehicles", *Washington, DC : National Highway Traffic Safety Administration.*, 261 pages, 2017.

[8] H. Berg, "Batteries for electric vehicles: Materials and electrochemistry", *Cambridge University Press*, 250 pages, 2015.

[9] S. J. Drake, D. A. Wetz, J. K. Ostanek, S. P. Miller, J. M. Heinzel and A. Jain, "Measurement of anisotropic thermophysical properties of cylindrical Li-ion cells", *Journal of Power Sources*, vol. 252, pp 298–304, 2014.

[10] X. Lin, H. E. Perez, S. Mohan, J. B. Siegel, A. G. Stefanopoulou, Y. Ding and M. P. Castanier, "A lumped-parameter electro-thermal model for cylindrical batteries", *Journal of Power Sources*, vol. 257, pp 1–11, 2014.

[11] T. S. Bryden, B. Dimitrov, G. Hilton, C. P. León, P. Bugryniec, S. Brown, D. Cumming and A. Cruden, "Methodology to determine the heat capacity of lithium-ion cells", *Journal of Power Sources*, vol. 395, pp 369–378, 2018.

[12] H. Zhou, F. Zhou, Q. Zhang, Q. Wang and Z. Song, "Thermal management of cylindrical lithium-ion battery based on a liquid cooling method with half-helical duct", *Applied Thermal Engineering*, vol. 162, 114257, 2019.

[13] J. Cao, M. Luo, X. Fang, Z. Ling and Z. Zhang, "Liquid cooling with phase change materials for cylindrical Li-ion batteries: An experimental and numerical study", *Energy*, vol. 191, 116565, 2020.

[14] S. Zhu, J. Han, H. Y. An, T. S. Pan, Y. M. Wei, W. L. Song, H. S. Chen and D. Fang, "A novel embedded method for in-situ measuring internal multi-point temperatures of lithium ion batteries", *Journal of Power Sources*, vol. 456, 227981, 2020.

[15] S. Zhu, J. Han, T. S. Pan, Y. M. Wei, W. L. Song, H. S. Chen and D. Fang, "A novel designed visualized Li-ion battery for in-situ measuring the variation of internal temperature", *Extreme Mechanics Letters*, vol. 37, 100707, 2020.

[16] C. Forgez, D. V. Do, G. Friedrich, M. Morcrette and C. Delacourt, "Thermal modeling of a cylindrical LiFePO4/graphite lithium-ion battery", *Journal of Power Sources*, vol. 195, pp 2961–2968, 2010.

[17] W. Zielenkiewicz and E. Margas, Theory of Calorimetry. Hot Topics in Thermal Analysis and Calorimetry, Springer Netherlands, 2002.

[18] P. M. Gomadam, R. E. White and J. W. Weidner, Theory of Calorimetry. "Modeling Heat Conduction in Spiral Geometries", *Journa of the Electrochemical Society*, pp A1339-A1345, 2003.

[19] T. S. Bryden, B. Dimitrov, G. Hilton, C. P. de León, P. Bugryniec, S. Brown, D. Cumming and A. Cruden, "Methodology to determine the heat capacity of lithium-ion cells", *Journal of Power Sources*, vol. 395, pp 369–378, 2018.

[20] K. A. Murashko, J. Pyrhönen and J. Jokiniemi, "Determination of the through-plane thermal conductivity and specific heat capacity of a Li-ion cylindrical cell", *International Journal of Heat and Mass Transfer*, vol. 162, 120330, 2020.

[21] Julabo USA Inc, "Data sheet for JULABO F25MA." `http://www.julabo.cn/uploadfile/2018/0411/JULABO-F25-MA--9153625.pdf`. [Accessed 16 October, 2020].

[22] Gamry Instruments, Inc., "Reference 3000 potentiostat/galvanostat/zra operator´s manual." `https://www.gamry.com/assets/Uploads/Reference-3000-Operators-Manual.pdf`, [Accessed 16 October, 2020].

[23] Pico technology, "PT-104 data logger." `https://www.picotech.com/download/datasheets/pt-104-prt-data-logger-data-sheet.pdf`, [Accessed 16 October, 2020].

[24] Kingspan Insulation AB, "Therma TW50 insulation plates information." `https://www.kingspan.com/se/sv-se/produkter/isolering/`

`therma/therma-tw50-skalmursisolering#`, [Accessed 17 October, 2020].

[25] L. C. Casals, B. A. García, F. Aguesse, and A. Iturrondobeitia, "Second life of electric vehicle batteries: relation between materials degradation and environmental impact," The International Journal of Life Cycle Assessment, vol. 22,no. 1, pp. 82–93, 2017

[26] IEEE, "Ieee code of ethics."http://www.ieee.org/about/corporate/governance/p7-8.html.

[27] G. Vertiz, M. Oyarbide, H. Macicior, O. Miguel, I. Cantero, P. F. de Arroiabe,and I. Ulacia, "Thermal characterization of large size lithium-ion pouch cellbased on 1d electro-thermal model," Journal of Power Sources, vol. 272, pp. 476– 484, 2014.

[28] Lidbeck, Anton and Syed, Kazim Raza "Experimental Characterization of Li-ion Battery Cells for Thermal Management in Heavy Duty Hybrid Applications", publications:lib.chalmers.se, Gothonburg,Sweden,Year 2017

[29] B. Löwen, S. Schulz, and J. Seippel, "Heat capacity measurement by calibration with dynamic correction of the calorimetric output signal of a thermopile heat¨conduction calorimeter," Thermochimica Acta, vol. 235, no. 2, pp. 147 – 152,1994.

[30] HBK Company, "X60 cold curing glue data sheet." `https://www.hbm.com/fileadmin/mediapool/support/safety-data-sheet/X60-A-from-2018/X60_-_A_USA-en.pdf`, [Accessed 20 October, 2020].

[31] S. Salicone, *Measurement Uncertainty*, *An Approach via the*, *Mathematical Theory of Evidence*. Springer Series in Reliability Engineering, 2007.

Bibliography

A
Appendix 1

A.1 Measurement variation calculations

For the calculations of variation for all the three thermal properties presented in this thesis, the standard deviation value was utilized to define the variation values. Considering a group with n samples, the standard deviation value (S) can be calculated as [31]

$$S = \sqrt{\sum_{i=1}^{n} \frac{(x_i - \overline{x})^2}{n}} \tag{A.1}$$

where $\overline{x}$ is the average value of the sample's group, n is the total number of samples and x_i represents each of the samples within the group. Lastly, the average value of a data group, composed by n samples, can be calculated as

$$\overline{x} = \sum_{i=1}^{n} \frac{x_i}{n} \tag{A.2}$$

A.1.1 Specific heat capacity (C_p)

For the calculation of the measurement variation regarding the cell's specific heat capacity, the samples presented in Table A.1 were utilized.

Table A.1: Utilized samples in the calculation of C_p measurement variation.

Sample index (i)	C_p [J/kg.ºC]
1	8.28E+02
2	8.70E+02
3	8.08E+02
4	8.57E+02
5	8.29E+02
6	8.52E+02
7	8.12E+02
8	8.62E+02
9	8.02E+02
10	8.85E+02

Applying the data set presented in Table A.1 into (A.1) and (A.2) resulted in $\overline{x} = \sum_{i=1}^{n} \frac{x_i}{n} = \frac{8.28 \times 10^2 + 8.70 \times 10^2 + ... + 8.85 \times 10^2}{10} = 8.41 \times 10^2 [\frac{J}{kg.°C}]$

$$S = \sqrt{\frac{(8.28 \times 10^2 - 8.41 \times 10^2)^2 + ... + (8.85 \times 10^2 - 8.41 \times 10^2)^2}{10}} = 27.1[\frac{J}{kg.°C}]$$

A.1.2 Axial thermal conductivity (K_a)

For the calculation of the measurement variation regarding the cell's axial thermal conductivity before adding the extra temperature sensor, the samples presented in Table A.2 were utilized.

Table A.2: Utilized samples in the calculation of K_a measurement variation.

Sample index (i)	K_a [W/m.K]
1	6.75
2	6.80
3	6.84
4	6.84
5	6.85
6	6.88
7	6.88
8	6.93
9	6.95
10	6.96
11	6.97
12	6.91
13	7.01
14	7.03
15	7.07
16	7.14

Applying the data set presented in Table A.2 into (A.1) and (A.2) resulted in

$$\bar{x} = \sum_{i=1}^{n} \frac{x_i}{n} = \frac{6.75 + 6.80 + ... + 7.14}{16} = 6.93[\frac{W}{m.K}]$$

$$S = \sqrt{\frac{(6.75 - 6.93)^2 + (6.80 - 6.93)^2 + ... + (7.14 - 6.93)^2}{16}} = 0.1[\frac{W}{m.K}]$$

Furthermore, the calculation of the measurement variation regarding the cell's axial thermal conductivity, considering the extra temperature sensor, were performed considering the samples presented in Table A.3.

Applying the data set presented in Table A.3 into (A.1) and (A.2) resulted in

$$\bar{x} = \sum_{i=1}^{n} \frac{x_i}{n} = \frac{11.67 + 11.71 + ... + 11.71}{16} = 11.55[\frac{W}{m.K}]$$

$$S = \sqrt{\frac{(11.67 - 11.55)^2 + (11.71 - 11.55)^2 + ... + (11.71 - 11.55)^2}{16}} = 0.1[\frac{W}{m.K}]$$

Table A.3: Utilized samples in the calculation of K_a measurement variation.

Sample index (i)	K_a [W/m.K]
1	11.67
2	11.71
3	11.73
4	11.74
5	11.71
6	11.35
7	11.39
8	11.40
9	11.41
10	11.42
11	11.44
12	11.71
13	11.47
14	11.49
15	11.45
16	11.71

A.1.3   Radial thermal conductivity (K_r)

For the calculation of the measurement variation regarding the cell's radial thermal conductivity, the samples presented in Table A.4 were utilized.

Table A.4: Utilized samples in the calculation of C_p measurement variation.

Sample index (i)	K_r [W/m.K]
1	0.79
2	0.84
3	0.87
4	0.89
5	0.85
6	0.77
7	0.78
8	0.78
9	0.82
10	0.84

Applying the data set presented in Table A.4 into (A.1) and (A.2) resulted in

$$\overline{x} = \sum_{i=1}^{n} \frac{x_i}{n} = \frac{0.79+0.84+...+0.84}{10} = 0.83[\frac{W}{m.K}]$$

$$S = \sqrt{\frac{(0.79-0.83)^2+(0.84-0.83)^2+...+(0.84-0.83)^2}{10}} = 0.04[\frac{W}{m.K}]$$